

Heat Transfer in Europa's Icy Shell

Amy C. Barr

Southwest Research Institute

Adam P. Showman

University of Arizona

Abstract: Heat transport across Europa's ice shell controls the thermal evolution of its interior and provides a source of energy to drive resurfacing. Recent improvements in knowledge of ice rheology, the behavior of convection, and the interaction between convection and lithospheric deformation have led to an increased level of realism and complexity in the study of the geodynamics of Europa's ice shell. The possibility of convection complicates efforts to determine the thickness of the ice shell: a thin conductive shell can carry the same heat flux as a thick convective shell. Whether convection occurs depends on ice viscosity, which in turn depends on grain size. The grain size may be controlled by internal deformation, or by impurities, depending on shell composition. Creating the observed surface features with steady-state thermal convection is challenging, even with tidal heating, because the near-surface ice is cold and stiff. Convection models that include surface weakening and compositional buoyancy show promise in explaining some chaos terrains, pits, and uplifts, but new spacecraft and laboratory data and geophysical techniques are needed to match theory to observation.

1. Introduction

Images of the surface of Europa returned by the *Galileo* spacecraft revealed that, in addition to its global network of linear features, portions of its surface are covered by pits, spots, uplifts, and chaos regions suggestive of convection-driven resurfacing (*Pappalardo et al. 1998; Greeley et al. 1998, 2004*). The implication that Europa's ice shell could be, or could have been convecting in the past, raised a number of questions about its geodynamical behavior: Can the shell convect at present? How does tidal dissipation affect the convection pattern? Can tidal dissipation and convection drive resurfacing? If the shell convects, can the ocean be thermodynamically stable? What role might compositional heterogeneity play in driving motion in Europa's ice shell?

30 The idea that solid-state convection may occur within Europa's icy shell dates to the
31 *Voyager* era when *Consolmagno and Lewis* (1978) suggested that the ice I layers of large
32 icy satellites could convect. *Reynolds and Cassen* (1979) determined that an ice shell on
33 Europa, Ganymede, or Callisto could convect if the shell were thicker than 30 km, and that
34 convection would rapidly freeze any liquid water ocean on a geologically short time scale.
35 In the decades since, advances in our knowledge about planetary convection, coupled with
36 laboratory experiments and field studies of ice deformation, have changed the way we think
37 about convection on Europa.

38 Recent laboratory and theoretical studies about the fluid-like behavior of solid water
39 ice have clarified the microphysical processes that accommodate deformation in ice (*Goldsby*
40 *and Kohlstedt* 2001; *Durham and Stern* 2001), and the processes that control grain size
41 (*McKinnon* 1999; *Schmidt and Dahl-Jensen* 2003; *Barr and McKinnon* 2007) and thus, vis-
42 cosity and tidal dissipation in Europa's ice shell. Application of numerical terrestrial mantle
43 convection models to Europa has shed light upon the conditions required to trigger con-
44 vection in Europa's shell (*McKinnon* 1999; *Ruiz and Tejero* 2003; *Barr et al.* 2004; *Barr*
45 *and Pappalardo* 2005), the behavior of the ice shell close to the onset of convection (*Mitri*
46 *and Showman* 2005, 2008a; *Solomatov and Barr* 2007), the behavior of tidal dissipation and
47 convection (*Tobie et al.* 2003; *Mitri and Showman* 2008b), the convective heat flux (*Freeman*
48 *et al.* 2006), the potential for convection-driven resurfacing (*Showman and Han* 2004, 2005;
49 *Han and Showman* 2008), and the potential for driving resurfacing with thermochemical
50 convection (*Pappalardo and Barr* 2004; *Han and Showman* 2005). Use of scaling relation-
51 ships between the physical properties of the ice shell, the critical Rayleigh number, and the
52 convective heat flux has helped constrain the conditions under which the ocean can avoid
53 freezing (*Hussmann et al.* 2002; *Freeman et al.* 2006; *Moore* 2006).

54 Despite these important advances, the modes of heat transfer across Europa's shell and
55 the link between heat transfer and resurfacing remain unclear. Direct numerical simulations
56 of convection-driven resurfacing cannot easily match the observed morphologies of pits, spots,
57 domes, and chaos – simulations find that thermal buoyancy stresses can create uplifts only

58 $\sim 1/10^{\text{th}}$ the height of those observed (*Showman and Han* 2004). Compositional convection
59 in a salty ice shell allows features with the correct heights to be explained (*Han and Showman*
60 2005), but determining whether convection can cause chaos formation remains a challenge
61 (*Showman and Han* 2005). Using the spacing between quasi-circular surface features on
62 Europa’s surface to constrain the physical properties, heat flux, and thermal structure of
63 the ice shell has proved problematic (e.g., *Nimmo and Manga* 2002). Compounding the
64 uncertainty, Europa’s shell may oscillate between a conductive and convective equilibrium,
65 wreaking havoc on its surface (*Mitri and Showman* 2005).

66 Here, we summarize recent breakthroughs in the understanding of solid-state convection,
67 numerical advances in modeling the coupled processes of tidal dissipation and convection,
68 and laboratory experiments clarifying the ductile behavior of ice. We discuss implications
69 of these advances for the modes of heat transport and resurfacing in Europa’s ice shell. In
70 §2, we provide an overview of heat sources and transport mechanisms in a tidally heated
71 ice shell. In §3, we review recent experiments clarifying how ice deforms in response to an
72 applied stress, which is long-standing source of uncertainty in european interior modeling. In
73 §4, we describe how the ice shell behaves close to the limit of convective stability. In §5, we
74 discuss how convection and tidal dissipation may contribute to the formation of Europa’s
75 rich variety of surface features including chaos, pits, spots, and uplifts.

76 2. Heat Generation and Transport

77 Europa’s ice shell is heated from beneath by radiogenic (and possibly tidal) heating
78 from its rocky core, and from within by tidal dissipation. Radiogenic heating within the
79 rocky core of Europa currently supplies roughly $F_r \approx (1/3)\rho H_r R_s (R_s / (R_s - z)) \sim 6$ to 8
80 mW m^{-2} to its surface heat flux, where $\rho = 3040 \text{ kg m}^{-3}$ is the mean density of Europa,
81 $H_r = (4.5 \pm 0.5) \times 10^{-12} \text{ W kg}^{-1}$ is the present chondritic heating rate (*Spohn and Schubert*
82 2003), $z \sim 120 \text{ km}$ is the thickness of Europa’s H_2O layer, and R_s is Europa’s radius.

83 The surface heat flux due to tidal dissipation in Europa (F_{tidal}) can be estimated as a

84 function of its physical and orbital properties,

$$85 \quad F_{tidal} = \frac{\dot{E}_{tidal}}{4\pi R_s^2} = \frac{21}{8\pi} \left(\frac{k_2}{Q} \right) \frac{R_s^3 G M_J^2 n e^2}{a^6}, \quad (1)$$

86 where \dot{E}_{tidal} is the tidal dissipation rate (Cassen *et al.* 1979, 1980), R_s is Europa's radius,
87 (k_2/Q) is the ratio between the degree-2 Love number (k_2) and the tidal quality factor (Q),
88 which describe how Europa's interior deforms in response to the jovian tidal potential, M_J
89 is the mass of Jupiter, $e = 0.01$ is Europa's orbital eccentricity, $n = 2\pi/P = 2.05 \times 10^{-5}$
90 s^{-1} is Europa's mean motion, and P is its orbital period. For a nominal value of $k_2 \sim 0.25$
91 (Moore and Schubert 2000) and $Q \sim 100$, $F_{tidal} \sim 10$ to 100 mW m^{-2} , larger than radiogenic
92 heating (Tobie *et al.* 2003; see also Sotin *et al.*, this volume).

93 How does Europa remove its tidal heat? The two possible heat transport mechanisms
94 within the outer ice I shell are conduction and solid-state convection. Figure 2a illustrates
95 the qualitative temperature structures that would accompany each of these states. In both
96 cases, the top layer has a steep, conductive temperature gradient; in the conductive case
97 (Fig. 2a, top), this layer extends to the top of the ocean, whereas in the convective case
98 (Fig. 2a, bottom), a thick, nearly isothermal ice layer lies underneath the conductive lid.
99 Despite greatly different thicknesses, these two solutions can potentially have similar surface
100 heat fluxes. This fundamental ambiguity makes it difficult to infer the ice shell thickness
101 from heat flow measurements. Here, we describe heat transport by conduction, and describe
102 the thermal structure of an ice shell that generates heat with tidal dissipation and removes
103 it by conduction. We then describe the governing equations of solid-state convection in
104 Europa's ice shell and define the fundamental quantities that describe a convecting ice shell,
105 including the Rayleigh number and Nusselt number. More detail about the behavior of a
106 convecting ice shell will be provided in §4 and §5.

107

2.1. Conduction

108 The simple estimate of how much tidal dissipation occurs in Europa from equation (1)
 109 provides us with an estimate of the heat flux carried across Europa’s outer ice I shell. If the
 110 ice shell is in conductive equilibrium, Fourier’s law relates the heat flux to the shell thickness,

$$111 \quad F_{cond} = \frac{k\Delta T}{D}, \quad (2)$$

112 where $\Delta T = T_b - T_s$ is the temperature difference between the temperature at its base
 113 (T_b), and its surface (T_s), and $k \sim 3.3 \text{ W m}^{-1} \text{ K}^{-1}$ (here assumed constant for simplicity)
 114 is a representative thermal conductivity for cold ice. The probable detection of an ocean
 115 beneath Europa’s ice (*Zimmer et al.* 2000) suggests that the base of the ice shell should be
 116 at the melting temperature of water ice (for pure water ice, $T_m = 253$ to 273 K at pressures
 117 relevant to Europa’s interior). The global average surface temperature on Europa is $T_s \sim 100$
 118 K (*Ojakangas and Stevenson* 1989). Setting $F_{cond} = F_{tidal}$ gives an ice shell thickness $D \approx 6$
 119 km (for $F_{tidal} \sim 100 \text{ mW m}^{-2}$) and $D \approx 60 \text{ km}$ (for $F_{tidal} \sim 10 \text{ mW m}^{-2}$).

120 The thermal conductivity is temperature-dependent; cold ice is a much better conductor
 121 of heat than warm ice (see *Petrenko and Whitworth* 1999 for discussion), so the temperature
 122 gradient close to the surface of the ice shell is steeper than at its base. The heat flux across
 123 a conductive ice shell with a temperature-dependent thermal conductivity is (cf. *Ojakangas*
 124 *and Stevenson* 1989),

$$125 \quad F = \frac{a}{D} \ln \left(\frac{T_b}{T_s} \right), \quad (3)$$

126 where $k = a/T$, and $a = 621 \text{ W m}^{-1}$ (*Petrenko and Whitworth* 1999).

127

2.2. A Tidally Heated Conductive Ice Shell

128 The most realistic models of tidal heating in Europa’s ice shell calculate the dissipation
 129 occurring in the shell due to its cyclical diurnal tidal flexure by modeling the ice shell as a
 130 Maxwell viscoelastic solid. For a general discussion of the Maxwell model, see *Ojakangas*

131 *and Stevenson (1989) and Turcotte and Schubert (2002)*. The energy dissipated in a Maxwell
 132 solid is maximized when the period of the forcing $T \sim \tau_M = \eta/\mu$, where τ_M is the Maxwell
 133 time, η is the viscosity, and μ is the shear modulus of the material. By coincidence (or orbital
 134 and geophysical “tuning” in the Jupiter system), the orbital period of Europa is very close
 135 to the Maxwell time for warm ice I ($\mu \sim 3.5 \times 10^9$ Pa and $\eta \sim 10^{15}$ Pa s, which gives $\tau_M \approx 3$
 136 days). A warm, internally heated ice shell on Europa ice shell may be close to a maximally
 137 dissipative state.

138 In a Maxwell viscoelastic solid, the volumetric dissipation rate (q) is proportional to
 139 viscosity, $q \sim \eta(T)\dot{\epsilon}^2$ at high temperatures and inversely proportional to viscosity, $q \sim$
 140 $\mu^2\dot{\epsilon}^2/(\omega^2\eta(T))$, at low temperatures. This implies a strongly temperature-dependent dissi-
 141 pation rate with peak dissipation occurring between ~ 220 and 270 K depending on the ice
 142 grain size (see below). A hot ice shell can therefore be more dissipative than a cold ice shell,
 143 and the dissipation should depend on the shell thickness (*Cassen et al. 1980*). This will
 144 affect the existence of equilibria between tidal dissipation and heat transfer.

145 To date, the most physically realistic model of a tidally heated conductive european ice
 146 shell was proposed by *Ojakangas and Stevenson (1989)*, who related the thickness of the ice
 147 shell, D , to the heat flux from the core H ,

$$148 \quad D \approx \frac{\ln(T_b/T_s)}{\left[\left(\frac{2}{a} \int_0^{T_b} \frac{q(T)dT}{T} + \left(\frac{H}{a} \right)^2 \right)^{1/2}}, \quad (4)$$

149 where $a = 621 \text{ W m}^{-1}$ (*Petrenko and Whitworth 1999*; see also equation 3). Physically, this
 150 equation describes a conductive equilibrium in an internally-heated ice shell with basal heat
 151 flux H and temperature-dependent thermal conductivity. If the ice is modeled as a Maxwell
 152 viscoelastic solid, the tidal dissipation rate is (*Ojakangas and Stevenson 1989*),

$$153 \quad q = \frac{2\mu\langle\dot{\epsilon}_{ij}^2\rangle}{\omega} \left[\frac{\omega\tau_M}{1 + (\omega\tau_M)^2} \right], \quad (5)$$

154 where $\langle\dot{\epsilon}_{ij}^2\rangle$ is the time-average of the square of the second invariant of the strain rate tensor,
 155 $\tau_M = \eta(T)/\mu$ is the temperature-dependent Maxwell time, and $\omega = n$. The dissipation rate

156 maximizes when $\omega \sim \tau_M$, corresponding to temperatures of $\sim 220\text{--}270$ K for ice viscosity of
 157 $\sim 10^{13}\text{--}10^{15}$ Pa s, close to plausible viscosities for warm ice (see discussion in §3). Equation
 158 (5) suggests that tidal dissipation occurs in the warmest ice, and that tidal dissipation in the
 159 cold, stiff portions of the ice shell is negligible. Assuming that the ice shell has horizontally
 160 uniform material properties, the quantity $\langle \dot{\epsilon}_{ij}^2 \rangle$ is a low-degree spherical harmonic function
 161 that varies by a factor of two between the minimum at the subjovian point and the maximum
 162 at the poles (see Figure 1 of *Ojakangas and Stevenson* 1989). The surface temperature on
 163 Europa also varies significantly, ranging from $T_s \sim 52$ K at the poles to $T_s \sim 110$ K at the
 164 equator. Integration of equation (4) with the tidal heat source (equation 5) and including
 165 the spatially varying surface temperature gives a the equilibrium ice shell thickness ranging
 166 from $\sim 15\text{--}30$ km as a function of location on Europa assuming radiogenic heating from the
 167 rocky core is 10 mW m^{-2} (*Ojakangas and Stevenson* 1989).

168 Since its development, spacecraft data and advances in our understanding of the behav-
 169 ior of a floating ice shell have questioned the applicability of the *Ojakangas and Stevenson*
 170 (1989) model. *Galileo* images of pits, chaos, and uplifts on Europa’s surface suggesting a con-
 171 vecting ice shell, and the suggestion that a shell $D \geq 30$ km thick could convect (*McKinnon*
 172 1999; see also §4) imply that the ice shell could be much thicker and still carry the tidal heat
 173 flux. The *Ojakangas and Stevenson* (1989) model, however, is an extremely valuable starting
 174 point for study of more complicated tidal/convective systems (e.g., *Tobie et al.* 2003) because
 175 it demonstrates that tidal dissipation in Europa’s shell is strongly rheology-dependent, and
 176 suggests that variations in tidal dissipation and surface temperature may lead to variations
 177 in the activity within the shell and potential for resurfacing.

178 2.3. Convection

179 Europa’s ice shell may also transport heat by solid-state convection. The density of
 180 water ice, like most solids, decreases as a function of increasing temperature. Therefore,
 181 an ice shell cooled from its surface and heated from within and beneath is gravitationally

182 unstable: warm ice rises, cold ice sinks, which transports thermal energy upward to the base
 183 of a conductive “lid” at the surface of the ice shell. When this process is self-sustaining over
 184 geologically long time scales, it is called solid-state convection.

185 Thermally driven convection in a highly viscous fluid with no inertial forces is described
 186 by the conservation equations for mass, momentum, and energy (cf. *Schubert et al.* 2001),

$$187 \quad \nabla \cdot \vec{v} = 0 \quad (6)$$

$$188 \quad \nabla p - \rho_o \alpha (T - T_o) g \hat{e}_z = \nabla \cdot [\eta (\nabla \vec{v} + \nabla^T \vec{v})] \quad (7)$$

$$189 \quad \vec{v} \cdot \nabla T + \frac{\partial T}{\partial t} = \kappa \nabla^2 T + H, \quad (8)$$

190 where \vec{v} is the velocity field, T is temperature, t is time, α is the coefficient of thermal expansion,
 191 T_o and ρ_o are reference values of density and temperature, κ is thermal diffusivity (here,
 192 assumed to be constant), p is the dynamic pressure (which excludes lithostatic pressure), \hat{e}_z
 193 is a unit vector in the vertical (z) direction, g is gravity, η is viscosity, and H represents heat
 194 sources.

195 In a shell where convection occurs, the heat flux, F_{conv} , is enhanced relative to the
 196 conductive heat flux by a factor of $Nu > 1$,

$$197 \quad F_{conv} = \frac{k \Delta T}{D} Nu, \quad (9)$$

198 where the Nusselt number, Nu , is related to the vigor of convection, expressed by the
 199 Rayleigh number,

$$200 \quad Ra = \frac{\rho_o g \alpha \Delta T D^3}{\kappa \eta}. \quad (10)$$

201 As we will describe in more detail in §4, convection can occur when the Rayleigh number
 202 of the ice shell exceeds a critical value, Ra_{cr} . The value of Ra_{cr} depends on how the ice
 203 viscosity varies with temperature and stress (*Solomatov* 1995; *Solomatov and Barr* 2006,
 204 2007). The relative efficiency of convective heat transport over conduction depends on the
 205 vigor of convection, an effect expressed in the relationship between Ra and Nu ,

$$206 \quad Nu = c Ra^{\beta_n}, \quad (11)$$

207 where the values of c and β_n depend on the variation in ice viscosity as a function of tem-
208 perature and stress (*Solomatov 1995; Dumoulin et al. 1999; Solomatov and Moresi 2000;*
209 *Freeman et al. 2006*) and (Ra/Ra_{cr}) , with extremely vigorous convection ($Ra \gg Ra_{cr}$) hav-
210 ing different c and β_n than sluggish convection ($Ra \gtrsim Ra_{cr}$) (*Dumoulin et al. 1999; Mitri*
211 *and Showman 2005*; see also §4.3). Thus, the possibility of convection and the efficiency of
212 convective heat transport depend critically on the viscosity of water ice and its variation as
213 a function of temperature and applied stress.

214 3. Ice Rheology and Grain Size

215 A large volume of laboratory experiments and field measurements exist regarding the
216 *rheology* of ice, meaning how solid ice flows in response to an applied stress. *Durham and*
217 *Stern (2001)* provide an excellent review of recent developments in this area. Here, we
218 focus on advances most relevant to Europa. We discuss the rheology of water ice and
219 the role of impurities in modifying the ice flow law and in controlling ice grain size. We
220 discuss control of ice grain size by secondary phases, dynamic recrystallization, and tidal
221 stresses. It should be noted that despite a number of important advances in the last decade,
222 the deformation mechanisms that accommodate large convective strains in Europa’s ice
223 shell and their descriptive parameters are still uncertain. Further laboratory experiments
224 characterizing the behavior of ice at conditions relevant to Europa’s ice shell are needed.

225 3.1. Rheology of Pure Water Ice

226 Over millions of years, solid water ice, like rock-forming minerals, can behave as a highly
227 viscous fluid. Solid ice is a polycrystalline material composed of individual grains; within
228 each grain, the orientation of the water crystal lattice is constant. Like all polycrystalline
229 solids, deformation in ice is accommodated by the motion of defects in the polycrystal,
230 either within grains, or along grain boundaries. A voluminous literature dating back to the

231 1900’s exists regarding the behavior of water ice, much of it developed by the glaciological
232 community who sought to understand the fluid-like behavior of ice observed in large ice
233 sheets and glaciers.

234 Ice rheology has traditionally been characterized in two regimes: a high-stress regime
235 (appropriate for glacial flow and the subject of considerable study in field and laboratory
236 settings), and a low-stress regime, wherein the relationship between stress and strain rate
237 has been estimated theoretically. Laboratory and glacial studies typically characterize ice
238 behavior at stresses between 10^{-2} and 10 MPa and strain rates between 10^{-7} s $^{-1}$ to 10^{-4}
239 s $^{-1}$ (*Durham and Stern* 2001). Typical convective strain rates on Europa are $\sim 10^{-13}$ s $^{-1}$
240 (*Tobie et al.* 2003), and stresses $\sim 10^{-3}$ MPa (*Tobie et al.* 2003; see also §3.1.1 here), so
241 some extrapolation to lower stresses and strain rates is required to apply laboratory or
242 field results to the study of satellite interiors. The rheology of ice at low stresses may be
243 appropriate for modeling deformation in the warm interiors of convecting ice shells. The
244 laboratory- and field-derived flow laws for ice I at high stresses are most appropriate for
245 modeling for example, the onset of convection, and lithospheric deformation. The boundary
246 between the “high” and “low” stress regimes depends on temperature and grain size (see
247 Figure 1). Both regimes of behavior may be relevant to calculating tidal dissipation, but
248 we note that the behavior of ice I undergoing cyclical deformation at European frequencies
249 is not well-characterized: further laboratory and field characterization is urgently needed to
250 advance our understanding of tidal heating.

251 3.1.1. Low Stress Regime: Diffusion Creep

252 The behavior of ice in the low-stress regime is relevant to modeling flow within the
253 warm regions of Europa’s ice shell ($T > 180$ K), in locations where the ice grain size is small
254 ($d < 1$ mm), and/or where the driving stresses are relatively low ($\sigma < 0.1$ MPa). Owing to
255 its low gravity, the thermal buoyancy stresses that drive motion within Europa’s ice shell
256 are small. Within the warm, well-mixed interior of a convecting ice shell, thermal buoyancy

257 stresses $\sigma_i \sim \rho g \alpha \Delta T_i \delta_{rh} \sim 10^{-3}$ MPa (equation 25 of *Solomatov and Moresi* 2000; see also
 258 *Tobie et al.* 2003), where $\Delta T_i \sim 10$ K is the magnitude of temperature fluctuations driving
 259 convection and δ_{rh} is the rheological boundary layer thickness (*Solomatov and Moresi* 2000),
 260 $\sim O(1\text{km})$. Like most rock-forming minerals, ice is thought to deform by diffusion creep
 261 at low stresses, high temperatures, and in materials with small grain size. Diffusion creep
 262 occurs by two processes: volume diffusion creep (Nabarro-Herring creep) and grain boundary
 263 diffusion creep (Coble creep) (*Goodman et al.* 1981),

$$264 \quad \dot{\epsilon}_{\text{diff}} = \frac{42V_m\sigma}{3RTd^2} \left(D_v + \frac{\pi\delta}{d} D_b \right), \quad (12)$$

265 where σ is differential stress, $R = 8.314$ J mol $^{-1}$ K $^{-1}$ is the gas constant, d is grain size,
 266 D_v is the rate of volume diffusion, $\delta = 2b$ is the grain boundary width, b is Burger's
 267 vector for ice, V_m is the molar volume, and D_b is the rate of grain boundary diffusion
 268 (*Goldsby and Kohlstedt* 2001). Each diffusion coefficient is strongly temperature-dependent,
 269 $D_v = D_{o,v} \exp(-Q_v/RT)$, and $D_b = D_{o,b} \exp(-Q_b/RT)$. Note also that the strain rate from
 270 diffusion creep is grain-size dependent.

271 To date, diffusion creep in ice has not been directly observed in laboratory experiments,
 272 so values of its governing parameters (summarized in Table I) are calculated based on micro-
 273 physical models of the diffusion processes. *Goodman et al.* (1981) provide a comprehensive
 274 discussion of diffusion processes in ice, section 5.5 of *Goldsby and Kohlstedt* (2001) gives
 275 recent updates for governing parameters, and *Goldsby* (2007) provides an update on efforts
 276 to observe diffusion creep in the laboratory. At conditions appropriate for a warm convecting
 277 ice shell with reasonable grain sizes ~ 0.1 mm to 1 mm, the deformation rate from diffusion
 278 creep is overwhelmingly dominated by the volume diffusion term. At $T > 258$ K, the rate of
 279 Coble creep in ice is expected to increase by a factor of 1000, due to pre-melting along grain
 280 boundaries and triple junctions, which allows for more efficient grain boundary diffusion
 281 than a purely solid grain boundary (*Goldsby and Kohlstedt* 2001). This results in a marked
 282 decrease in the viscosity of ice within 10 K of the melting point (see deformation maps of
 283 *Durham and Stern* 2001), an effect which has been largely overlooked in current numerical
 284 studies (with the noted exception of *Tobie et al.* 2003).

285 An effective viscosity can be calculated from the stress-strain rate relationship (*Durham*
 286 *and Stern* 2001; *Ranalli* 1987),

$$287 \quad \eta = \frac{1}{3^{(n+1)/2}} \frac{\sigma}{\dot{\epsilon}}, \quad (13)$$

288 where the factor of $3^{(n+1)/2}$, where n is the rheological stress exponent, is included because
 289 the stresses that drive deformation have not been resolved into shear and normal components
 290 (*Ranalli* 1987). For diffusion creep, $n = 1$. This gives an effective viscosity due to volume
 291 diffusion,

$$292 \quad \eta_{\text{diff}} = \frac{RTd^2}{42V_m D_{o,v}} \exp\left(\frac{Q_v^*}{RT}\right). \quad (14)$$

293 The resulting behavior of ice is said to be “Newtonian”, meaning that the effective viscosity
 294 is independent of stress, and that stress and strain rate are linearly related. The volume
 295 diffusion flow law and variants of it have been widely applied to study of the interior of
 296 Europa’s ice shell since the 1980’s. It is common to re-write the flow law as,

$$297 \quad \eta = \eta_o \exp\left[A\left(\frac{T_m}{T} - 1\right)\right], \quad (15)$$

298 which is equivalent to equation (14) if $A = Q^*/RT_m \sim 26$ for pure water ice and η_o is equal
 299 to $\eta_{\text{diff}}(d_o, T_m)$, where d_o is an assumed grain size. The value η_o is commonly assumed to
 300 be a free parameter ranging from $\eta_o \sim 10^{13}$ to 10^{15} Pa s, corresponding to grain sizes of 0.1
 301 mm and 1 mm, respectively (using equation 14). The volume diffusion rheology has been
 302 used in all existing calculations of tidal dissipation within Europa’s ice shell (*Ojakangas*
 303 *and Stevenson* 1989; *Tobie et al.* 2003; *Showman and Han* 2004; *Mitri and Showman* 2005,
 304 2008b). We note that, at the stresses associated with Europa’s daily tidal flexing, ~ 0.1
 305 MPa, or during the onset of convection, non-Newtonian deformation mechanisms could be
 306 relevant (*Barr et al.* 2004).

307 *3.1.2. High Stress Regime: GSS and Dislocation Creep*

308 The behavior of ice I at relatively high stresses $\sigma > 0.01$ MPa is well-characterized by
 309 laboratory experiments and glacial measurements. Although the stresses in a convecting

310 ice shell on Europa are relatively low, larger stresses ($\sigma \sim 0.01$ MPa) may build up in the
 311 ice shell during the onset of convection (see §4.2.1) or by lithospheric deformation. In ice
 312 with a grain size $d > 1$ mm, flow driven by stresses of this magnitude is accommodated by
 313 dislocation creep and grain-size-sensitive creep.

314 In this regime, the stress-strain rate relationship for water ice is described as,

$$315 \quad \dot{\epsilon} = \frac{B}{d^p} \sigma^n \exp\left(\frac{-Q^*}{RT}\right) \quad (16)$$

316 where B and n are constants determined in laboratory experiments, or from measuring
 317 glacial flow, and p is the grain size exponent. A summary of flow laws determined between
 318 1952 and 1979 by *Weertman* (1983) reveals the level of uncertainty in ice rheology during the
 319 *Voyager* era. Values of n ranging from 1.6 to 4 had been measured in different contexts: creep
 320 in polycrystalline ice at low temperature (perhaps most appropriate for Europa) suggested
 321 $n \sim 3$ and activation energies between 60 to 80 kJ mol⁻¹ (*Weertman* 1983). Because
 322 $n > 1$, the effective ice viscosity in the high-stress regime depends on stress (i.e., ice is
 323 “non-Newtonian” meaning that strain rate depends non-linearly on stress).

324 Laboratory experiments reveal that for $\sigma > 1$ MPa, deformation in ice occurs by dislo-
 325 cation creep, characterized by equation (16) with $n = 4$ and $Q^* = 60$ kJ mol⁻¹ (*Goldsby and*
 326 *Kohlstedt* 2001). Dislocation creep has a high stress exponent $n = 4$, so the strain rate in
 327 cold ice with a large grain size depends strongly on the applied stress (i.e., the ice is highly
 328 non-Newtonian) and its strain rate is independent of grain size. Similar to the low-stress
 329 regime, strain rates from dislocation creep in ice with $T > 258$ K are also increased due to
 330 premelting at grain boundaries and three- and four-grain junctions in ice (see section 5.4 of
 331 *Goldsby and Kohlstedt* (2001)).

332 Recent laboratory experiments suggest the existence of an intermediate regime for 0.01
 333 MPa $< \sigma < 1$ MPa (see Figure 5 of *Goldsby and Kohlstedt* (2001)), wherein deformation
 334 occurs by weakly non-Newtonian deformation mechanism(s) referred to collectively as “grain-
 335 size-sensitive” (GSS) creep. GSS creep is characterized by a relatively low stress exponent
 336 $n \sim 2$, a relatively low grain size exponent $1 < p < 2$, and a modest activation energy

337 $Q^* \sim 49 - 60 \text{ kJ mol}^{-1}$ (*Goldsby and Kohlstedt 2001; Durham et al. 2001*). GSS creep
 338 is of particular interest to the glacial community, because most large ice bodies on Earth,
 339 which have grain sizes ~ 1 to 10 mm and driving stresses ~ 0.1 MPa, are deforming in the
 340 intermediate stress regime.

341 Although the governing parameters of GSS creep are generally agreed upon, identifi-
 342 cation of the specific microphysical process that accommodate strain in this regime is an
 343 open area of debate. The values of the governing parameters strongly suggest that easy slip
 344 (equivalently basal slip), where ice grains deform along the basal planes of their hexagonal
 345 crystals, occurs in the intermediate regime (*Goldsby and Kohlstedt 2001; Duval et al. 2000*).
 346 A secondary process such as dislocation creep or grain boundary sliding must operate in
 347 tandem with basal slip to accommodate deformation in crystals whose planes are not ori-
 348 ented properly for basal slip to occur (*Goldsby and Kohlstedt 2002*). The identification of
 349 this secondary process has been problematic. Scanning electron microscopy of deformed ice
 350 samples allowed *Goldsby and Kohlstedt (2001)* to identify instances of grain switching and
 351 occurrence of straight grain boundaries and four-grain junctions, providing evidence that
 352 grain boundary sliding accommodates easy slip. This gives rise to a combined flow law in
 353 the intermediate regime (*Goldsby and Kohlstedt 2001*),

$$354 \quad \dot{\epsilon}_{\text{gss}} = \left(\frac{1}{\dot{\epsilon}_{\text{gbs}}} + \frac{1}{\dot{\epsilon}_{\text{bs}}} \right)^{-1}, \quad (17)$$

355 where *gbs* stands for grain boundary sliding, and *bs* stands for basal slip, with the strain
 356 rate from grain boundary sliding ($\dot{\epsilon}_{\text{gbs}}$) dominating at conditions relevant to the interior
 357 of Europa's ice shell (*Barr et al. 2004*). Governing parameters for GSS creep effectively
 358 controlled by GBS are summarized in Table I. However, it has been suggested that grain
 359 boundary sliding and basal slip acting together are not able produce the crystal fabric (the co-
 360 alignment of crystal lattices in adjacent grains) observed in deformed sections of terrestrial
 361 ice sheets (*Duval et al. 2000; Duval and Montagnat 2002*). *Montagnat and Duval (2000)*
 362 suggest an alternate hypothesis: that grain boundary migration (essentially, grain growth)
 363 and associated recrystallization accommodates basal slip. However *Goldsby and Kohlstedt*
 364 (*2002*) point out that grain boundary migration does not produce strain and thus is not

365 a deformation mechanism. The identification of the microphysical process accommodating
366 deformation in ice at moderate stresses remains an active area of research.

367 3.1.3. A Combined Flow Law

368 *Goldsby and Kohlstedt* (2001) propose that the behavior of ice I across the high, inter-
369 mediate, and low-stress regimes can be described by a single governing equation,

$$370 \dot{\epsilon}_{\text{total}} = \dot{\epsilon}_{\text{diff}} + \dot{\epsilon}_{\text{gss}} + \dot{\epsilon}_{\text{disl}}, \quad (18)$$

371 where, in application to Europa’s ice shell, the strain rate due to GSS may be approximated
372 by the governing parameters of grain boundary sliding (*Barr et al.* 2004). Despite uncertain-
373 ties in the microphysical mechanisms at work in GSS creep, a combined flow law including
374 both GSS and dislocation creep using governing parameters summarized in Table I provides
375 a good match to stress/strain rate/grain size relationships deduced from previous laboratory
376 experiments (*Goldsby and Kohlstedt* 2001) and glacial measurements (*Peltier et al.* 2000).
377 The composite flow law can be used to determine the regimes of dominance in stress, tem-
378 perature, and grain size space for each constituent deformation mechanism. By equating
379 strain rates between pairs of mechanisms, one can construct a deformation map for ice that
380 can be used to predict which rheology is appropriate for a given application (see Figure 1
381 and deformation maps of *Durham and Stern* (2001)).

382 3.2. Effect of Impurities

383 The presence of substances other than water ice in Europa’s ice shell can have an
384 important effect on its rheology. Here we summarize how the presence of various materials,
385 including ammonia, sulfate salts, and dispersed particulates, may affect the rheology of
386 Europa’s ice shell.

387 Ammonia dihydrate, $\text{NH}_3 \cdot 2\text{H}_2\text{O}$, the stable phase in the water-rich, low pressure region

388 of phase space in the ammonia-water system, melts at $T_m = 176$ K. Ammonia has been
389 suggested as a possible means to thermodynamically stabilize liquid water oceans beneath
390 convecting ice shells (e.g., *Spohn and Schubert* 2003) and implicated as a possible component
391 of cryovolcanic magmas on icy satellites. The rheology of ammonia dihydrate has been
392 measured in laboratory experiments by *Durham et al.* (1993). The flow law for ammonia
393 dihydrate, with mole fraction $x_{NH_3} = 0.3$ (corresponding to a mole fraction of 90% dihydrate)
394 can be expressed in similar form as equation (16), with $B = 10^{-15} \text{ Pa}^{-5.8} \text{ s}^{-1}$, $n = 5.8$,
395 and $Q^* = 102 \text{ kJ mol}^{-1}$. At its melting point and a nominal stress of 0.01 MPa, ammonia
396 dihydrate is two orders of magnitude less viscous than water ice, but its large activation
397 energy leads to a rapid increase in viscosity as the temperature is decreased.

398 *Galileo* NIMS data suggest that the surface of Europa's ice shell is composed predom-
399 inantly of water ice and nonice materials that include one or more hydrated materials.
400 Candidates for the latter include hydrated magnesium and/or sodium salts *McCord et al.*
401 (1999) or hydrated solidified sulfuric acid (*Carlson et al.* 2005). Geochemical modeling of
402 water-rock chemistry in Europa's ocean also suggest the formation of magnesium and/or
403 sodium salts, supporting the view that the ice shell may be salty throughout (*Zolotov and*
404 *Shock* 2001; *McKinnon and Zolensky* 2003). The sulfate salts were found to have much
405 higher viscosities than pure water ice at comparable temperatures (*Durham et al.* 2005). For
406 example, the difference in hardness between mirabilite grains and water ice is so high that
407 the dispersed mirabilite particles can act as hard secondary phases, and have a similar effect
408 on the rheology of the bulk material as silicate grains.

409 Recent laboratory experiments by, e.g., *McCarthy et al.* (2007) have explored dissipation
410 in mixtures of ice and magnesium sulfate. Frozen eutectic mixtures of ice and magnesium
411 sulfate form a lamellar structure with layers of ice and magnesium sulfate sandwiched to-
412 gether. The resulting mixture is stiff but highly dissipative due to the micro-scale boundaries
413 between layers of magnesium sulfate and water ice. Future laboratory experiments on pure
414 water ice and water ice mixed with other materials may provide alternate models for dissi-
415 pation than the Maxwell model, and help bridge the gap between theory and data regarding

416 tidal dissipation in Europa.

417 Europa’s ice shell may contain small amounts of silicate dust, but the dust content is
418 limited by its bulk density – the ice shell must maintain a low enough density to remain
419 gravitationally stable atop the $\rho \sim 1000 \text{ kg m}^{-3}$ ocean (or more if the ocean is salty). Small
420 rock particles (with sizes much less than the mean ice grain size) mixed with ice act as a
421 barrier to flow within the ice and disturbs the flow pattern – as a result, the effect of particles
422 on ice viscosity depends critically upon the location of the particles within the polycrystalline
423 structure of ice. Laboratory experiments characterizing the viscosity of mixtures of ice with
424 a grain size of $\sim 1 \text{ mm}$ and silicate particles with grain sizes $\sim 100 \mu\text{m}$ show that the increase
425 in viscosity of water ice due to the presence of SiO_2 and SiC/SiCaCO_3 grains at low volume
426 fractions relevant to Europa’s ice shell, $\phi < 0.1$, is negligible (see Figure 14 of *Durham et al.*
427 (1992)). However, silicate particles may play a role in inhibiting grain growth in Europa’s
428 ice shell, as will be discussed in §3.3.1.

429 **3.3. Ice Grain Size**

430 Observations of grain size and the processes that control grain size in terrestrial ice
431 sheets experiencing stress and temperature conditions similar to the interior of Europa’s ice
432 shell can provide estimates of likely grain sizes. Grain sizes in Europa’s shell are commonly
433 assumed to be uniform and between 0.1 mm to 10 mm, by analogy with grain sizes in
434 terrestrial ice sheets (*Budd and Jacka* 1989; see also, e.g., *Thorsteinsson et al.* (1997) for a
435 sample ice core grain size profile).

436 Two recent works cast doubt upon these estimates and have led to a reevaluation of
437 the plausibility of the 0.1 to 10 mm range for assumed ice grain sizes. *Nimmo and Manga*
438 (2002) estimated the viscosity at the base of the ice shell by using the measured diameters of
439 pits and uplifts ($\sim 4\text{--}10 \text{ km}$) to infer properties of the underlying convection pattern. They
440 obtained a basal viscosity for the ice shell between 10^{12} to 10^{13} Pa s , and suggested that ice
441 grain sizes at the base of the shell should be between 0.02 and 0.06 mm. Follow-on studies

442 by *Showman and Han* (2004) suggest that near-surface ice grain sizes less than 0.04 mm are
443 required to create small depressions such as those observed on the surface of Europa (see
444 §5.1). *Schmidt and Dahl-Jensen* (2003) applied a simple model of unimpeded grain growth
445 in the low-stress, high-temperature, and liquid-rich environment at the base of Europa’s ice
446 shell and suggested that its grain size may be between 4 cm to 80 meters. Because the rate
447 of volume diffusion depends on grain size squared, the range of ice viscosity implied by all
448 the above estimates is 15 orders of magnitude.

449 However, the estimates of *Schmidt and Dahl-Jensen* (2003) ignore processes known
450 to modify grain sizes within terrestrial ice cores. In addition, the geodynamical studies
451 did not account for near-surface weakening by other processes (e.g., microcracking), which
452 could explain the low effective near-surface viscosity required to create depressions, or the
453 possibility of pre-melting at the base of Europa’s ice shell, which could yield low basal
454 viscosities for a much larger grain size. Because stress and temperature conditions expected
455 within Europa’s ice shell are similar to those experienced by many ice bodies on Earth,
456 processes controlling grain sizes within terrestrial ice sheets may control grain size within
457 Europa’s ice shell and act to self-regulate and/or limit its ice grain size to values closer to
458 those observed in ice cores. Here, we discuss two possible methods of controlling ice grain
459 size in Europa’s ice shell: 1) Zener pinning due to the presence of hard secondary phases
460 (*Kirk and Stevenson* 1987; *Barr and McKinnon* 2007), and 2) dynamic recrystallization/tidal
461 flexing (*McKinnon* 1999; *Barr and McKinnon* 2007).

462 3.3.1. Grain Size Control by Secondary Phases

463 Measured grain sizes in many terrestrial ice cores indicate that grain size in impurity-
464 laden ice are invariably smaller than those in clean ice (*Alley et al.* 1986a,b). In the absence
465 of impurities, grains grow by grain boundary migration driven by the free energy decrease
466 associated with reduction of grain boundary curvature. Non-water-ice materials concentrate
467 on grain boundaries, and can decrease the grain growth rate and in some cases can even

468 halt grain growth altogether (*Poirier* 1985; *Alley et al.* 1986a,b). The role that any type
 469 of impurity plays in inhibiting or preventing grain growth depends on the location of the
 470 impurity within the structure of the ice polycrystal: impurities concentrated along grain
 471 boundaries and at grain junctions can be much more effective at inhibiting grain growth
 472 than impurities randomly dispersed in the ice (*Durand et al.* 2006). Recent advances in SEM
 473 imaging of samples from ice cores shows the spatial correlation between silicate microparticles
 474 and kinks in grain boundaries, providing compelling evidence that silicate particles can
 475 inhibit grain growth (*Weiss et al.* 2002).

476 On Europa, one could imagine that silicate or salt particles might act as hard secondary
 477 phases (or pinning particles) that could slow or halt grain growth. The effect of pinning
 478 particles on grain size was modeled by Zener, who related the drag force exerted by hard
 479 secondary phases on grain boundaries to the rate of grain growth dr/dt (*Poirier* 1985),

$$480 \quad \frac{dr}{dt} = K_{g,0} \exp\left(\frac{-E_A}{RT}\right) \left(\frac{1}{r} - \frac{P_Z}{\alpha_G \gamma_{gb}}\right) \quad (19)$$

481 where $E_A = 46 \text{ kJ mol}^{-1}$ is the activation energy for grain boundary migration, $\gamma_{gb} = 0.065$
 482 J m^{-2} is the grain boundary free energy (*De La Chapelle et al.* 1998), and $\alpha_G = 0.25$ is a
 483 geometric factor. The pinning pressure P_Z exerted on the grain boundary is related to the
 484 number of particles on the boundary (fN_x) (*Poirier* 1985) (where f is the number fraction
 485 of particles residing on the grain boundary), $P_Z = \frac{1}{3}\pi\gamma_{gb}r_x r fN_x$, where r_x is the radius of the
 486 particles residing on the grain boundary and N_x is the number of particles per unit volume.
 487 Grain growth is completely stopped when $dr/dt = 0$, which gives the Zener limiting grain
 488 size (cf. *Durand et al.* 2006),

$$489 \quad r_z = \left(\frac{3\alpha_G}{\pi r_x f N_x}\right)^{1/2}, \quad (20)$$

490 where the numerical factor of 3 indicates that the particles reside on grain boundaries, and
 491 $f \sim 0.25$ is estimated by counting the number of particles residing on grain boundaries in
 492 SEM images of the GRIP ice core (*Barnes et al.* 2002; *Weiss et al.* 2002). If we suppose that
 493 the ice shell of Europa is loaded with microscopic silicate particles of density 3000 kg m^{-3}
 494 and radii of 10 microns, up to a total volume percentage of 4%, the Zener limiting grain size

495 is

$$496 \quad r_z = 0.1 \text{ mm} \left(\frac{r_x}{10 \text{ } \mu\text{m}} \right) \left(\frac{0.04}{\phi} \right)^{1/2}, \quad (21)$$

497 where ϕ is the volume fraction of silicate in Europa's ice shell, and $N_x \sim \phi / (\frac{4}{3}\pi r_x^3)$. The
498 upper limit on ice grain size derived from the Zener pinning model is inversely proportional
499 to impurity content – fewer impurities mean larger grain sizes. We note that *Kirk and*
500 *Stevenson* (1987) constructed a similar argument to estimate grain sizes in the ice mantle of
501 Ganymede: their estimate has a similar dependence on radii of the silicate particles and the
502 volume fraction of silicate in the ice shell. For Europa, we can put a plausible estimate on
503 the upper limit of silicate content based on the density of the ice shell – if the shell density
504 exceeds 1000 kg m^{-3} (or more for a salty ocean), it will be gravitationally unstable atop the
505 ocean.

506 Observations of grain sizes between 0.5 to 1 mm in impurity-laden sections of terrestrial
507 ice cores, coupled with our upper limit on ice grain size based on a Zener pinning model
508 suggest that grain sizes in Europa's ice shell may hover around the 0.1 to 1 mm range (*McK-*
509 *innon* 1999; *Barr and McKinnon* 2007). At present, terrestrial observations of grain growth
510 and impurity distribution within polycrystalline ice are limited to temperatures between
511 235 to 273 K. Therefore, knowledge of grain size and processes controlling grain size gained
512 through study of terrestrial cores may be most applicable to the warm and convecting inte-
513 rior ice shell (*Barr and McKinnon* 2007). Grain sizes closer to the surface of Europa may
514 be controlled by other, non-thermally activated processes such as cyclical tidal deformation
515 (*McKinnon* 1999).

516 3.3.2. *Dynamic Recrystallization*

517 Observations of relatively impurity-free sections of terrestrial ice cores reveal that ice
518 grain sizes are constant as a function of depth (equivalently, time) within sections of the
519 core that have experienced significant strain (*Thorsteinsson et al.* 1997; *De La Chapelle*
520 *et al.* 1998). If ice grains can grow unimpeded, one would expect grain size in the ice

521 sheet to increase as a function of depth and time. This suggests that deformation acts to
 522 decrease grain size, thereby competing with natural grain growth and allowing a roughly
 523 constant steady-state grain size to be maintained over time. It has been suggested that the
 524 accumulated strain due to vertical layer compaction results in grain size reduction due to
 525 a process called dynamic recrystallization (*Thorsteinsson et al. 1997; De La Chapelle et al.*
 526 *1998*). In dynamic recrystallization, the grain size in a deforming material is controlled by
 527 a balance between grain growth and the formation of new grains (nucleation) by a process
 528 called subgrain rotation (*Shimizu 1998; De Bresser et al. 1998*). Subgrain rotation can only
 529 occur if deformation is occurring in the material, leading to a threshold strain at which grain
 530 sizes in a deforming material achieve their steady-state recrystallized values. For temperature
 531 and strain rate conditions appropriate for the GRIP ice core, $T \sim 240$ K and $\dot{\epsilon} \sim 10^{-12}$ s $^{-1}$,
 532 the threshold strain is about 25% (*Thorsteinsson et al. 1997*). A model of this process
 533 has been applied to estimate grain sizes within actively deforming regions of ice shells by
 534 *Barr and McKinnon (2007)*, who find that in the well-mixed, warm convective interior of an
 535 already convecting ice shell, grain sizes will evolve to a steady-state value that depends on
 536 the applied stress (*Derby 1991; Shimizu 1998; De Bresser et al. 1998; Barr and McKinnon*
 537 *2007*),

$$d_{recrys} = Kb \left(\frac{\sigma}{\mu} \right)^{-m}, \quad (22)$$

538
 539 where $K = 1-100$ is a grouped material parameter, μ is the ice shear modulus, and $m = 1.25$.
 540 *Barr and McKinnon (2007)* suggest that in the absence of impurities, recrystallized grain
 541 sizes in convecting ice shells will be large, $d_{recrys} \sim 30$ to 80 mm, leading to highly viscous
 542 ice and a gradual shut-down of convection as the grains achieve their recrystallized value.
 543 The implication is that without impurities to limit grain growth, ice shells may convect
 544 sluggishly, and be limited to a small number of convective overturns before transitioning to
 545 a conductive state.

546 On Europa, however, tidal flexing of the ice shell itself may control the ice grain size.
 547 *McKinnon (1999)* hypothesized that if cyclical straining in the presence of convection of
 548 Europa's ice shell has the same effect as the continuous strain on terrestrial ice cores (i.e.,

549 driving dynamic recrystallization), the grain size in the ice shell would decrease as $d \propto \dot{\epsilon}^{-1/2}$.
550 The grain size controlled in this manner would have a *maximum* of 1 mm at the warm base
551 of the ice shell. Thus, cyclical tidal flexing may prevent grains in Europa’s ice shell from
552 growing to the large values predicted by continuous-deformation dynamic recrystallization
553 models (*Barr and McKinnon 2007*), exempting Europa’s ice shell from being choked while
554 convecting.

555 4. Ice Shell Convection

556 In §2, we described two possible modes of removing tidal heat generated in Europa’s ice
557 shell: conduction and convection. But how do we decide whether convection can happen?
558 Until recently, knowledge of how convection starts and stops in realistic planetary mantles
559 was relatively limited because terrestrial planet mantles are commonly assumed to convect
560 throughout most of their geologic history. Although many of the techniques developed
561 for studying terrestrial planet mantle convection apply to Europa, the heat flow history in
562 Europa’s ice shell sets it apart from terrestrial planets. Unlike a terrestrial planetary mantle,
563 Europa’s ice shell may receive periodic bursts of heat due to tidal dissipation in addition
564 to radiogenic heating from its rocky core. As a result, the mode of heat transport across
565 Europa’s ice shell may change from conductive to convective many times during its evolution
566 (*Mitri and Showman 2005*). Here, we summarize several decades’ worth of study of the issue
567 of whether convection is possible in Europa’s ice shell, how convection may start and stop,
568 and the efficiency of convective heat transport.

569 4.1. Is Convection Possible?

570 Early efforts to judge whether convection could happen in Europa’s ice shell used two
571 implicit assumptions. First, it was assumed that deformation during the onset of convection
572 would be accommodated by Newtonian diffusion creep, even though field and laboratory

573 measurements of ice viscosity suggested that ice could be non-Newtonian if the grain size
574 is sufficiently large. It was also assumed that the value of the critical Rayleigh number
575 was independent of the type of temperature perturbations available to trigger convection in
576 the ice shell. Here, we discuss the consequences of relaxing these assumptions. Recently
577 developed numerical techniques allow for the study of how convection may be triggered from
578 “realistic” temperature fluctuations in the ice shells; we summarize the results of these
579 studies.

580 The simplest representation of Europa’s ice shell in the language of fluid dynamics is
581 a layer of fluid cooled from above and heated from within and beneath. It is common to
582 assume that a conductive ice shell on Europa is heated mostly at its base by radiogenic and
583 tidal heating because tidal dissipation is likely maximized there (however, this assumption
584 is not necessarily correct; see §5.2.1). It is also common to model the ice shell as using a
585 2-D Cartesian geometry. Although Europa’s ice shell is, truly, a spherical shell, plausible
586 ice shell thicknesses are small compared to the radius of Europa, so for many purposes it is
587 sufficient to think of it as a Cartesian box. At present, most simulations of convection in
588 Europa’s ice shell are performed in 2-D because of limited computing resources.

589 The question of whether convection can occur in a fluid layer has been studied in a
590 variety of planetary and fluid dynamical contexts. It is a simple geophysical argument: does
591 the Rayleigh number of the fluid layer exceed a critical value? Using the definition of the
592 Rayleigh number (equation 10), this can be phrased mathematically as,

$$593 \quad \frac{\rho g \alpha \Delta T D^3}{\kappa \eta} \geq Ra_{cr}, \quad (23)$$

594 where Ra_{cr} is the critical Rayleigh number. The value of Ra_{cr} for convection in any fluid
595 depends on the wavelength of initial temperature perturbation within the fluid layer and
596 the geometry of the layer (see *Turcotte and Schubert* (2002) for discussion). Because both
597 the thickness of Europa’s ice shell and its viscosity are poorly constrained at present, we
598 cannot definitively determine whether convection can occur: the best we can do is determine

599 a critical shell thickness where convection is possible by rearranging equation (23),

$$600 \quad D_{cr} = \left(\frac{Ra_{cr} \kappa \eta}{\rho g \alpha \Delta T} \right)^{1/3}, \quad (24)$$

601 and constrain values of D_{cr} as a function of physical properties of the ice shell.

602 *4.1.1. Newtonian Viscosity*

603 Early works such as that of *Consolmagno and Lewis* (1978) and *Reynolds and Cassen*
604 (1979) approximated ice as a constant-viscosity fluid. In a constant viscosity fluid, $Ra_{cr} \approx$
605 1000 (*Chandrasekhar* 1961), so estimates of the mean ice viscosity, thermal and physical
606 parameters, and the surface temperature and ice melting temperatures on Europa could be
607 used to determine D_{cr} from equation (24) alone. *Reynolds and Cassen* (1979) determined
608 that convection could occur in a bottom-heated ice I shell on a Europa-like satellite if $D \gtrsim 30$
609 km.

610 A source of uncertainty in evaluating D_{cr} for a constant-viscosity ice shell is the appro-
611 priate choice of viscosity value. The viscosity of ice is strongly temperature-dependent, so
612 do we evaluate D_{cr} using $\eta(T_s)$, or $\eta(T_m)$ or some well-chosen mean? This is addressed using
613 algebraic (“scaling”) relationships between the activation energy in the ice flow law (which
614 controls $\partial\eta/\partial T$) and the critical Rayleigh number for a Newtonian fluid by *Stengel et al.*
615 (1982) (for $n = 1$) and *Solomatov* (1995) (for general n).

616 The analysis of *Solomatov* (1995) focuses on the behavior of the bottom thermal bound-
617 ary layer of a basally heated fluid with a strongly temperature-dependent viscosity at the on-
618 set of convection. If the viscosity of the fluid depends strongly on temperature (if $\eta(T_s)/\eta(T_m) \gtrsim$
619 10^4 (*Solomatov* 1995)), fluid motions in the upper part of the layer are miniscule, and the
620 upper part of the layer forms a lid of cold, high-viscosity fluid (referred to as a “stagnant”
621 lid). In the so-called “stagnant lid regime”, convective fluid motions are confined to a warm
622 sublayer at the base of the fluid, where the temperature is approximately constant, and the
623 temperature dependence of ice viscosity can be neglected. With this approximation, the

critical Rayleigh number for convection in a fluid with a temperature-dependent viscosity can be estimated by determining when the warm sublayer begins to convect, or determining when the *local* Rayleigh number in the sublayer exceeds 1000. The result is a scaling relationship between the critical Rayleigh number and rheological parameters of the fluid (Solomatov 1995),

$$Ra_{1,cr} = Ra_{cr}(n) \left[\frac{e\theta}{4(n+1)} \right]^{2(n+1)/n}, \quad (25)$$

where the subscript 1 indicates that we will compare this critical Rayleigh number to the Rayleigh number at the base of the ice shell (where $T = T_b$), n is the rheological stress exponent, $\theta = \gamma\Delta T$, where the Frank-Kamenetskii parameter, $\gamma = -\partial(\ln \eta)/\partial T|_{T_i} = Q^*/(RT_i^2)$, and $Ra_{cr}(n) \approx Ra_{cr}(1)^{1/n} Ra_{cr}(\infty)^{(n-1)/n}$. In icy satellite convection studies, it is commonly assumed that the warm, well-mixed convective interior of the ice shell has a temperature very close to the ice melting point, so $T_i \approx T_b = T_m$. This gives $\theta \approx (Q^*\Delta T)/(RT_m^2)$ (cf. McKinnon 2006). The value $Ra_{cr}(n)$ represents the critical Rayleigh number for convection in a fluid with a viscosity dependent solely on stress (i.e., $\eta = B\sigma^n$), which is estimated using the value for $n = 1$, $Ra_{cr}(1) = 1568$ and the limit of $Ra_{cr}(n)$ as $n \rightarrow \infty$, or $Ra_{cr}(\infty) \approx 20$ (see Figure 5 of Solomatov 1995).

A large volume of work exists regarding the onset of convection in ice I shells of the satellites assuming a Newtonian rheology for ice: in these studies the viscosity of ice depends strongly on temperature, but is independent of stress. For a Newtonian ice rheology, $n = 1$, and equation (25) reduces to (Stengel *et al.* 1982; Solomatov 1995),

$$Ra_{1,cr} = 20.9\theta^4. \quad (26)$$

A surface temperature of $T_s = 100$ K and basal temperature of $T_m = 260$ K implies $\theta \approx 18$, which gives $Ra_{cr,1} = 2.2 \times 10^6$ (using equation (26)). Values of $Ra_{cr,1}$ for a range of θ values appropriate for volume diffusion and Europa's ice shell are summarized in Table II. Evaluating equation (24) using $\rho = 920$ kg m⁻³, $\kappa = 2.6 \times 10^{-6}$ m² s⁻¹ as a representative value for warm ice, and evaluating the ice viscosity using coefficients in the volume diffusion flow law (see Table I), gives an expression for the critical shell thickness for convection (cf.

651 *McKinnon* 1999),

$$652 \quad D_{cr,diff} = 31 \text{ km} \left(\frac{d}{0.4 \text{ mm}} \right)^{2/3}, \quad (27)$$

653 where the nominal value of $d = 0.3 \text{ mm}$ gives a basal ice viscosity of 10^{14} Pa s , mid-way
654 between the values of 10^{13} to 10^{15} Pa s commonly assumed in Europa studies.

655 *4.1.2. Realistic Ice Rheology*

656 For ice with small grain sizes $d \lesssim 1 \text{ mm}$, diffusion creep likely accommodates strain
657 during the onset of convection, and the critical ice shell thickness for convection is given
658 by equation (27). However, the composite flow law for ice suggests that deformation at
659 stresses built up within ice shells during the onset of convection may be accommodated
660 by non-Newtonian GSS creep (*Barr et al.* 2004). If convection is triggered by temperature
661 fluctuations of $\delta T \sim 5 \text{ K}$ and height $\lambda \sim D$, the thermal stress due to a plume of this
662 magnitude is approximately $\sigma_{th} \sim \rho g \alpha \delta T \lambda \sim 0.02 \text{ MPa}$. For grain sizes $\gtrsim 1 \text{ mm}$, strain
663 due to stresses of order σ_{th} may be accommodated by GSS creep (see Figure 1). When GSS
664 creep accommodates deformation during the onset of convection,

$$665 \quad D_{cr} = \left(\frac{Ra_{a,1} (\kappa d^p)^{(1/n)} \exp\left(\frac{Q^*}{nRT_m}\right)}{(3^{(n+1)/2} A)^{1/n} \rho g \alpha \Delta T} \right)^{n/(n+2)} \quad (28)$$

666 where $Ra_{a,1} = 3.1 \times 10^4$ is the absolute minimum Rayleigh number where convection is
667 possible (for an optimal perturbation) in GBS with $\theta \approx 15$ appropriate for an ice shell with
668 $T_s = 90 \text{ K}$ and $T_m = 260 \text{ K}$ (*Barr and Pappalardo* 2005). Equation (28), which is for arbitrary
669 n and can be used for non-Newtonian fluids, reduces to equation (24) for $n = 1$. Evaluating
670 the rheological parameters for GSS using the grain boundary sliding values (see Table I),
671 and using nominal values for descriptive properties of the ice shell, the critical shell thickness
672 becomes,

$$673 \quad D_{cr,GSS} = 75 \text{ km} \left(\frac{d}{1 \text{ mm}} \right)^{1.4/3.8}. \quad (29)$$

674 The grain size at which GSS becomes the “controlling” rheology at the onset of con-
675 vection can be determined by setting equations (27) and (29) equal and solving for d . This
676 gives $d = 2$ mm, indicating that in ice with a grain size ≤ 2 mm, diffusion creep likely
677 accommodates strain during the onset of convection. For $d > 2$ mm, GSS creep accommo-
678 dates strain during the onset of convection. Figure 2b summarizes how the critical ice shell
679 thickness where convection can occur depends on ice grain size and an ice shell with a realistic
680 Newtonian diffusion creep and non-Newtonian GSS rheology (*Barr and Pappalardo* 2005).

681 *McKinnon* (1999) argues that tidal stresses in Europa’s ice shell may alter its rheology.
682 In an ice shell deforming by GSS creep, if the tidal stresses are much greater than the
683 thermal buoyancy stresses driving convection, the GSS viscosity law can become effectively
684 “linearized”. The effect is similar to the modification of mantle rheology due to interaction
685 between convection and post-glacial rebound on Earth (*Schmeling* 1987). Within Europa’s
686 ice shell, the low-stress convective flow field “sees” an effectively Newtonian rheology, but
687 the high-stress tidal field “sees” a non-Newtonian viscosity. *McKinnon* (1999) estimates a
688 basal viscosity of 8×10^{13} Pa s for tidally linearized GBS, which depends on grain size as
689 $\eta \propto d^{1.4/1.8}$. Convection is possible in a 25 km-thick ice shell with such a rheology if the grain
690 size is about 1 mm, which may be the case if grain size is controlled by tides (see §3.3.2).

691 Here, we have calculated critical ice shell thicknesses for convection assuming a constant
692 thermal conductivity for the ice shell. The critical ice shell thickness for convection in a
693 variable-conductivity shell is larger than in a constant-conductivity shell. This effect can be
694 estimated by equating the equivalent heat flow F_{conv} across a shell with variable conductivity
695 to F_{conv} with a constant conductivity (*McKinnon* 1999, 2006; *Tobie et al.* 2003; *Barr and*
696 *Pappalardo* 2005; see also equations 2 and 3).

$$697 \quad \frac{D_{true}}{D_{cr}} = \frac{a}{k_c \Delta T} \ln \left(\frac{T_m}{T_s} \right), \quad (30)$$

698 where D_{true} is the actual critical shell thickness with variable conductivity taken into account,
699 D_{cr} is the value obtained assuming a constant conductivity of k_c (here, $3.3 \text{ W m}^{-1} \text{ K}^{-1}$).
700 For $T_s = 100$ and $T_m = 260$ K, $D_{true}/D_{cr} \sim 1.17$.

701 Finally, we note that although it is beyond the scope of this chapter, it is possible that
702 the microphysical processes that accommodate the first $\sim 10\%$ strain during the onset of
703 convection are entirely different than those that govern well-developed convection (see e.g.,
704 *Birger* (1998, 2000)). Measurements of ice behavior during transient or primary creep (*Glen*
705 1955) may be relevant to the question of the onset of convection in addition to flow laws for
706 steady-state creep (*Solomatov and Barr* 2007).

707 Amazingly, the results of recent efforts to refine the range of ice shell thicknesses gener-
708 ally agree with the original estimates of the critical shell thickness for convection derived by
709 *Reynolds and Cassen* (1979): $D_{cr} \sim 30$ km. Although the *value* of critical ice shell thickness
710 may not have changed much in 30 years, the relationship between ice rheology, the critical
711 shell thickness for convection, and ice grain size has been clarified.

712 4.2. Behavior of the Ice Shell Close to the Critical Rayleigh Number

713 4.2.1. Starting Convection

714 In the previous section, we described the results of recent studies attempting to narrow
715 the range of conditions where convection is *possible* in Europa's ice shell. In a mathematically
716 idealized scenario, an unperturbed and heated ice shell will sit quiescently unless temperature
717 fluctuations drive flow and trigger convection. Since the earliest work on convective stability,
718 it has been known that the critical Rayleigh number depends on the shape (e.g., *Turcotte*
719 *and Schubert* 2002) and amplitude of temperature perturbation within the fluid layer (see,
720 e.g., *Chandrasekhar* (1961), *Stengel et al.* (1982) for discussion).

721 A key open question in the study of Europa's ice shell is whether tidal dissipation can
722 trigger convection in the shell. Because the Maxwell time of warm ice near the base of
723 Europa's shell may be close to Europa's orbital period, a purely conductive ice shell may
724 be heated largely at its base. Recent numerical work suggests that maximally effective
725 perturbations for starting convection are concentrated at the base of the fluid layer and

726 have wavelength $\lambda_{cr} \sim 2(n + 3)\theta^{-1}D$ (Solomatov and Barr 2006, 2007). In the absence of
727 temperature fluctuations, zones of weakness, or other means of localizing tidal dissipation,
728 tidal heating in a conductive ice shell is essentially constant over the horizontal scale of
729 convective cells because the r.m.s. strain rate varies by only a factor of ~ 2 between the
730 equator to pole. One could envision the temperature perturbation due to tidal dissipation
731 as a smoothly-varying harmonic function with a wavelength $\lambda_{tidal} \sim R_{Europa}/4$ or so (see
732 Figure 1 of Ojakangas and Stevenson 1989). If tidal heating is the sole cause of the density
733 differences necessary to trigger convection, tidal dissipation must generate temperature per-
734 turbations on horizontal length scales $\lambda \sim \lambda_{cr}$ to trigger convection (Barr et al. 2004). If
735 $\lambda_{tidal} \gg \lambda_{cr}$, the critical Rayleigh number would increase substantially, perhaps by a factor
736 of 100 or more, because perturbations with such long wavelengths are inefficient at triggering
737 convection. This suggests that tidal dissipation, as envisioned by Ojakangas and Stevenson
738 (1989) may not be able to trigger convection in a *purely* conductive ice shell.

739 Other types of temperature fluctuations, for example, bursts of heat released close to
740 the surface of the ice shell from large impacts are essentially useless in triggering convection
741 because they diffuse away too quickly to warm the surrounding ice enough to permit it to flow.
742 Compositional variations present in a realistic ice shell may be able to provide the necessary
743 density contrasts to trigger convection (e.g., Pappalardo and Barr 2004). Understanding
744 how convection begins in Europa’s ice shell will require characterization of the types and
745 locations of temperature fluctuations naturally present in the ice shell.

746 4.2.2. Stopping Convection

747 If the Rayleigh number of Europa’s ice shell drops below the value where convection can
748 be maintained, convection will cease. The Ra of the ice shell may change, for example, due to
749 perturbations in the basal heat flux (Mitri and Showman 2005), or due to an increase in ice
750 grain size over time (Barr and McKinnon 2007). Gray arrows in Figure 2c describe the path
751 in Ra - Nu space taken by an ice shell where convection is stopping. As the Rayleigh number is

752 decreased, Nu decreases until $Ra = Ra_{cr}^*$, the lowest value of Ra where convection is possible.
753 For Newtonian rheologies in the stagnant lid regime ($\theta > 8$), the value of $Ra_{cr}^* \sim \frac{1}{2}Ra_{cr,1}$ (see
754 Table II). In the vicinity of this point, $(Nu - Nu_{cr}) \propto (Ra - Ra_{cr})^{1/2}$, and at $Ra = Ra_{cr}^*$,
755 $Nu \approx 1.1$ to 1.3 , and convective motion is confined to a very thin layer at the base of the
756 ice shell. Values of Ra_{cr}^* and $Nu(Ra_{cr}^*)$ for a range of parameters appropriate for a volume
757 diffusion rheology and range of θ appropriate for Europa's ice shell are summarized in Table
758 II (see also Table 1 of *Solomatov and Barr (2007)*). When convection stops, very low values
759 of $(Nu - 1)$ can be achieved, and the minimum value scales with θ^{-1} (*Solomatov and Barr*
760 *2007*).

761 4.2.3. Convective/Conductive Switching

762 When convection starts in an ice shell, it results in a reorganization of heat and mass
763 transfer in its interior. The spatially averaged temperature in the shell increases significantly,
764 as does the heat flux across the shell, resulting in thermal stresses that may be sufficient to
765 drive lithospheric deformation (*Mitri and Showman 2005*). Here, we summarize the results
766 of these recent studies about convective turn-on and turn-off in an ice shell with a Newtonian
767 rheology, and discuss implications for resurfacing of Europa's ice shell.

768 The black arrows in Figure 2c describe the path in $Ra - Nu$ space traced out by a
769 Newtonian ice shell during the onset of convection. From a conductive equilibrium ($Nu = 1$),
770 the ice shell begins convecting when $Ra = Ra_{cr,1}$ (see equation 25), and the heat flux jumps
771 rapidly to $Nu > 1$ (*Mitri and Showman 2005*; *Solomatov and Barr 2007*). Values of Nu
772 achieved for $Ra = Ra_{cr,1}$ using a volume diffusion rheology for ice and numerical methods
773 described by *Solomatov and Barr (2007)* are summarized in Table II.

774 The value of Nu achieved during the onset of convection depends on the type of tem-
775 perature perturbation that exists or develops in the conductive ice shell (*Solomatov and*
776 *Barr 2007*). As described in §4.2.1, the most efficient perturbations at starting convection
777 are confined to the base of the ice shell: the optimal perturbation shape (for stagnant lid

778 convection in a 2D Cartesian geometry) is a small convective roll obtained for $Ra = Ra_{cr}^*$
 779 (see §4.2.2). Using the optimal perturbation shape gives a lower bound on the jump in heat
 780 flux when convection begins; for $\theta = 18$, Nu jumps from 1 to 1.56 when convection begins.
 781 Using a sinusoidal perturbation that adds $\delta T = 0.175$ to a background conductive equilib-
 782 rium, *Mitri and Showman* (2005) find that Nu jumps to 1.7 in a tidally heated ice shell.
 783 The difference between the two values provides an estimate of the effect of perturbation
 784 geometry on the ΔNu associated with the onset of convection: ΔNu changes by $\sim 20\%$ as
 785 the wavelength is varied by a factor of ~ 2 . This suggests that careful consideration of the
 786 types of realistic temperature perturbations available to trigger convection in icy satellites
 787 is required to obtain more accurate estimates of the heat flux jump when convection begins.

788 A $Nu(Ra)$ plot, as shown in Figure 2c, is the most straightforward way of summarizing
 789 the heat flux across an ice shell during the onset and decay of convection. To understand the
 790 geological consequences of the onset of convection, we need to trace variations in the heat
 791 flux as a function of ice-shell thickness. For Europa, this is most easily done by assuming
 792 that the viscosity at the base of the ice shell (i.e., the melting-temperature viscosity) is
 793 independent of shell thickness; the Rayleigh number can then be directly translated into a
 794 measure of shell thickness. Likewise, with equation (2) we can translate Nu into heat flux.
 795 Figure 2d shows an example of such a plot, from *Mitri and Showman* (2005), assuming the
 796 melting-temperature viscosity is 10^{13} Pa sec. The existence of a heat flux jump implies that,
 797 for a range of heat fluxes relevant to Europa (basal heat fluxes between $35\text{--}60\text{ mW m}^{-2}$ in
 798 this case), two solutions exist for a given heat flux — a thin conductive shell and a thick
 799 convective shell (*Mitri and Showman* 2005). Modest variations in the heat flux can force the
 800 shell to switch between these states. This will have important geophysical consequences.

801 Imagine a thin, conductive ice shell, with its basal temperature held at the local melting
 802 temperature of water ice, which is in steady-state with an enormous basal heat flux. Imagine
 803 that this basal heat flux gradually declines in time. Such a system would begin in the upper
 804 left corner of Figure 2d and would gradually slide down the conductive branch toward the
 805 right as the shell slowly thickened. When the shell reaches 8 km thickness at a basal heat

806 flux of 35 mW m^{-2} (for the parameters in Figure 2d), a crisis ensues: the critical Rayleigh
807 number is reached and convection initiates, but the convection transports far more heat flux
808 than is available from below. Thus, the shell cannot continue to thicken while remaining
809 in equilibrium. Instead, rapid thickening occurs until the shell reaches a new equilibrium
810 thickness of $\sim 15 \text{ km}$ at the heat flux of 35 mW m^{-2} . Any continued reductions in the basal
811 heat flux lead to continued shell thickening on the convective branch. Conversely, suppose
812 the shell lies on the convective branch and experiences a gradually increasing basal heat flux.
813 The shell can gradually thin, maintaining equilibrium, until reaching a thickness of $\sim 9 \text{ km}$
814 at a basal flux of 60 mW m^{-2} . Again, a crisis ensues: the shell cannot continue to thin while
815 maintaining equilibrium with the heat flux available from below. Instead, the shell becomes
816 conductive, and then transports far less heat than is available from below. Melting ensues,
817 which rapidly thins the shell until a new conductive equilibrium is attained at a thickness of
818 $\sim 5 \text{ km}$ at the basal flux of 60 mW m^{-2} .

819 Thus, the heat-flux jump implies that modest variations in the basal heat flux can lead
820 to large, and geologically rapid, changes in the ice shell thickness. These thickness changes
821 occur over a timescale (*Mitri and Showman 2005*)

$$822 \quad \tau \approx \frac{L\rho\Delta D}{\Delta F} \approx 10^7 \text{ years} \quad (31)$$

823 where $L \approx 3 \times 10^5 \text{ J kg}^{-1}$ is the latent heat, $\Delta D \approx 10 \text{ km}$ is the thickness change resulting
824 from the conductive/convective transition, and $\Delta F \approx 20 \text{ mW m}^{-2}$ is the mismatch in fluxes
825 between the heat flux transported by the ice shell and that supplied from below. Import-
826 tantly for tectonics, this timescale is much shorter than typical orbital and thermal evolution
827 timescales of 10^8 – 10^9 years.

828 These rapid changes in shell thickness cause rapid changes in Europa’s volume, which
829 can lead to stresses up to $\sim 10 \text{ MPa}$ and may induce surface fracture (*Mitri and Showman*
830 *2005; Nimmo 2004*). Thus, conductive-convective switches may have important implications
831 for European tectonics. The fact that Europa’s heat flux could vary episodically (*Hussmann*
832 *and Spohn 2004*) opens the possibility that such conductive-convective switches may have
833 occurred repeatedly in Europa’s history.

834

4.3. Convective Heat Flux

835 As introduced in §2.3, the relationship between the convective heat flux and the vigor
 836 of convection can be expressed in a relationship of form, $Nu = cRa^{\beta_n}$. For convection in a
 837 fluid with a temperature-dependent viscosity, the value of c depends on θ (*Solomatov* 1995),
 838 giving rise to a $Ra - Nu$ relationship of form (cf. *Solomatov and Moresi* 2000),

$$839 \quad Nu = a\theta^{-\alpha_n} Ra_i^{\beta_n} \quad (32)$$

840 where a , α_n and β_n are constants that depend on n , and Ra_i is the value of Rayleigh
 841 number evaluated at T_i (and additionally, a strain rate of κ/D^2 for a non-Newtonian rheology,
 842 *Solomatov and Moresi* 2000). Scalings between Nu and Ra_i can be used for both internally
 843 heated and basally heated ice shells provided T_i is properly estimated in the basally heated
 844 case (described in detail by *McKinnon* 2006).

845 For steady convection in a Newtonian fluid at low Ra , (for $Ra/Ra_{cr} \lesssim 10^3$), *Dumoulin*
 846 *et al.* (1999) suggest $a = 1.99$, $\alpha_n = 1$ and $\beta_n = 1/5$. For vigorous convection, where the
 847 velocity and temperature field are time-dependent ($Ra/Ra_{cr} \gtrsim 10^3$), *Solomatov and Moresi*
 848 (2000) suggest $a = (0.31 + 0.22n)$, $\alpha_n = 2(n + 1)/(n + 2)$, and $\beta_n = n/(n + 2)$, which
 849 for Newtonian ice, where $n = 1$, give $a = 0.53$, $\alpha_n = 4/3$, and $\beta_n = 1/3$. Numerical
 850 simulations of vigorous convection with a multi-component rheology for water ice including
 851 terms from Newtonian diffusion creep and weakly non-Newtonian GBS give $a = (0.82 \pm 1.69)$,
 852 $\alpha_n = 1.07 \pm 0.19$, and $\beta_n = 0.25 \pm 0.02$, which are roughly similar to the values for diffusion
 853 creep alone (*Freeman et al.* 2006). The applicability of these relationships to tidally heated
 854 ice shells with viscosity-dependent tidal dissipation has not yet been demonstrated explicitly.
 855 However, it is likely that the coefficients in the $Ra - Nu$ relationship for tidally heated ice
 856 shells will be similar to those derived for uniform internal heating (e.g., *Solomatov and*
 857 *Moresi* 2000). Because tidal dissipation in the cold stagnant lid at the surface of the ice
 858 shell is negligible (*Showman and Han* 2004), viscosity-dependent tidal heating does not
 859 fundamentally alter the value of θ , the behavior of the stagnant lid, or the rheological
 860 boundary layer between the stagnant lid and the well-mixed convective interior of the ice

861 shell, which are the key controls on Nu (Solomatov and Moresi 2000; Barr 2008).

862

5. Convective-driven Resurfacing

863

864

865

866

867

868

869

870

871

872

873

874

875

Galileo observations showed that Europa's mottled terrain consists predominantly of chaos terrains, pits, domes, platforms, irregular uplifts, and lobate features (Carr *et al.* 1998; Pappalardo *et al.* 1998; Greeley *et al.* 1998; Greenberg *et al.* 1999, 2003). Although several formation mechanisms have been suggested, including melt-through of the ice shell (Greenberg *et al.* 1999; O'Brien *et al.* 2002; Melosh *et al.* 2004) and cryovolcanism (Fagents 2003), the most common suggestion is that these features formed from subsurface convection in the ice shell (Pappalardo *et al.* 1998; Collins *et al.* 2000; Head and Pappalardo 1999; Spaul 2002; Spaul *et al.* 2004; Figueredo *et al.* 2002; Figueredo and Greeley 2004). More generally, tectonic features on Enceladus, Miranda, Triton, and other moons have also been suggested to result, directly or indirectly, from subsurface convection (e.g., Nimmo and Pappalardo 2006; Pappalardo *et al.* 1997; Schenk and Jackson 1993). Here we review our current understanding of the extent to which subsurface convection can induce surface tectonics on icy satellites.

876

877

878

879

880

881

882

883

884

885

886

Two basic routes exist whereby convection may modify a planetary surface. First, the convective stresses and strains below the lithosphere (associated with the convective temperature and motion fields) could directly cause surface fracture and deformation. Candidates for this type of *direct* modification include Europa's chaos, pits, and uplifts; Triton's cantaloupe terrain, and Miranda's coronae. Second, the effects of convection on the internal density structure and long-term evolution could lead, indirectly, to non-convective stresses that induce surface tectonics. For example, time variation in convective density anomalies could lead to reorientation of the satellite figure relative to the rotation axis; substantial surface stresses would occur as the rotational and tidal bulges shifted across the surface. This may be relevant to Enceladus (Nimmo and Pappalardo 2006). Alternately, convection could lead to changes in the thickness of the ice shell, and hence in satellite volume, leading to

887 global tensional or compressional stresses. This mechanism is potentially relevant to Europa,
888 Ganymede, and other bodies (*Nimmo* 2004; *Mitri and Showman* 2005, 2008a; see also §4.2).

889 Here, we focus on the first mechanism and discuss the extent to which convection can
890 produce surface features such as pits, uplifts, and chaos terrains. This problem has been at-
891 tacked with a variety of approaches, ranging from simplified analytical calculations (*Rathbun*
892 *et al.* 1998; *Nimmo and Manga* 2002) to full numerical simulations of the convection (*Sotin*
893 *et al.* 2002; *Tobie et al.* 2003; *Showman and Han* 2004, 2005; *Han and Showman* 2005, 2008).
894 We first address the production of topography (pits and uplifts) and second discuss surface
895 disruption (chaos).

896 5.1. Pits and uplifts

897 A difficulty in explaining large-amplitude topography and surface disruption by con-
898 vection is the small expected convective stresses on icy satellites (*Showman and Han* 2004).
899 Thermal-buoyancy stresses associated with convective plumes are $\sigma \sim \rho \alpha g h \delta T$, where ρ , α ,
900 and g are density, thermal expansivity, and gravity; δT is the temperature difference between
901 a plume and its surroundings, and h is the vertical height of the plume. The temperature-
902 dependent viscosity leads to the development of a stagnant lid at the surface; the convection
903 then occurs in a nearly isothermal sublayer confined below the stagnant lid. Theoretical
904 studies imply that the total viscosity contrast across such a sublayer is only a factor of ~ 10
905 (e.g., *Solomatov and Moresi* 2000), which for realistic activation energies (Q^*) implies that
906 convective plumes have temperature contrasts of only ~ 10 K. As emphasized by *Showman*
907 *and Han* (2004, 2005), this weak thermal buoyancy leads to small stresses of only ~ 0.01 MPa
908 (*Tobie et al.* 2003; see also §3.1.1). The dynamic (i.e., convectively generated) topography
909 induced by such stresses is only $\sigma/\rho g \sim 10$ m (*Nimmo and Manga* 2002; *Showman and*
910 *Han* 2004), which is far below the ~ 100 – 300 m heights of typical European uplifts. These
911 stresses are also much less than the expected yield stress of ice, suggesting that pure thermal
912 convection cannot easily fracture the surface.

913 Several authors have performed analytical calculations of the conditions required to
914 explain the properties of pits and uplifts by convection. *Rathbun et al.* (1998) adapted a
915 simple model for the ascent of hot thermal diapirs through a cooler ice shell to study the
916 formation of uplifts in Europa’s shell. Based on the fact that diapirs spread laterally as they
917 impinge against the stagnant lid, *Rathbun et al.* (1998) suggested that the initial diapirs must
918 have diameters of several km or less to explain uplifts ~ 10 km across. They also suggest
919 that, to remain coherent as they ascend, such diapirs must have originated from depths
920 less than ~ 30 km. Using boundary-layer theory, *Nimmo and Manga* (2002) carried these
921 arguments further by linking such diapiric behavior to the required convective properties of
922 the ice shell. Hot ascending diapirs presumably originate in the hot convective boundary
923 layer at the bottom of the ice shell, and experimental results show that the initial diapir
924 diameter is ~ 5 times the thickness of the bottom hot boundary layer (*Manga and Weeraratne*
925 1999). Based on this result, *Nimmo and Manga* (2002) infer that the bottom boundary
926 layer thickness needed to explain 10 km-diameter domes is ~ 1 –2 km. This demands a small
927 melting-temperature viscosity of 10^{12} – 10^{13} Pa s, implying ice grain sizes of only 0.02–0.06 mm
928 (see §3.3) *Nimmo and Manga* (2002) also suggest that, for such a diapir to induce surface
929 uplift, the stagnant lid thickness must be < 2 –4 km, implying heat fluxes of 100–200 mW m $^{-2}$.
930 Consistent with the buoyancy arguments described above, their predicted dome heights are
931 only ~ 5 –30 m, far less than the observed heights of typical European domes.

932 Although the above analytical studies are valuable, they adopted simplified prescriptions
933 of the dynamics that potentially exclude important effects. To determine whether pit-and-
934 dome-like surface topography can result from the full convective dynamics, *Showman and*
935 *Han* (2004) performed two-dimensional numerical simulations using a diffusion creep rhe-
936 ology. (We note that use of a non-Newtonian rheology does not modify the fundamental
937 buoyancy argument described above and is unlikely to, by itself, lead to convection-driven
938 resurfacing). *Showman and Han* (2004) found that, in stagnant-lid convection, ascending
939 and descending plumes have essentially no surface expression — pits and uplifts do not form
940 (see Figure 3). This results directly from the extremely small temperature contrasts (~ 10 K)

941 of the ascending and descending plumes. The simulations developed modest surface topogra-
942 phy of $\sim 10\text{--}30$ m, which resulted from long-wavelength lateral variations in the thickness of
943 the stagnant lid rather than from the plumes underlying the lid. *Showman and Han* (2004)
944 found, however, that if the viscosity contrast is $\Delta\eta \sim 10^3\text{--}10^5$, then the cold ice at 1–2-km
945 depth deforms enough to participate in the convection ($\Delta\eta$ is small enough that convection
946 occurs in the so-called “sluggish lid” regime), leading to formation of 100–300 m-deep pits
947 over the downwellings. However, none of the simulations produced localized uplifts. The
948 simulated pits range in width from 5–100 km depending on the melting-temperature viscos-
949 ity, thickness of the ice shell, and other properties. Consistent with *Nimmo and Manga*
950 (2002), *Showman and Han* (2004) found that explaining observed pits with diameters of
951 $\sim 5\text{--}10$ km requires melting-temperature viscosities of $\sim 10^{12}$ Pa s or less, implying ice grain
952 sizes of ≤ 0.04 mm. At these viscosities, the maximum heat flux transportable by convection
953 is $\sim 100\text{--}150$ mW m $^{-2}$. Explaining pits less than ~ 4 km in diameter is extremely difficult
954 unless the viscosities are unrealistically small.

955 Runaway tidal heating in hot convective plumes is sometimes invoked as a mechanism
956 for enhancing the internal temperature contrasts and, therefore, increasing the amplitude of
957 surface topography. However, *Showman and Han* (2004) pointed out that such runaways, if
958 any (see §5.2.1), cannot significantly enhance the thermal buoyancy in ascending hot plumes.
959 The mean ice temperature in the convective sublayer is only ~ 10 K less than the temperature
960 at the bottom of the ice shell, which for Europa is expected to be the ~ 260 K melting
961 temperature. Even accounting for the pressure-dependence of the melting temperature,
962 this puts a fundamental limit of $\sim 10\text{--}20$ K on the maximum temperature difference between
963 ascending hot plumes and the background ice through which they rise: plumes simply cannot
964 be heated to temperatures exceeding the melting temperature. Once a hot plume reaches
965 the melting temperature, any further heating will instead cause partial melting, which would
966 increase the plume’s density and therefore *decrease* its thermal buoyancy — lessening the
967 topographic amplitude of any resulting uplifts.

968 Motivated by the insufficient buoyancy associated with *thermal* density contrasts, several

969 authors have proposed that *compositional* density contrasts are important in generating the
970 large (100–300 m) topography of typical pits and uplifts (*Showman and Han* 2004; *Pappalardo*
971 *and Barr* 2004; *Nimmo et al.* 2003; *Han and Showman* 2005). The most plausible scenario
972 for explaining uplifts is one where relatively salt-free (hence low-density) diapirs ascend
973 through a saltier, denser environment. In this case the topography is $\sim h\Delta\rho/\rho$, where
974 $\Delta\rho$ is the plume-environment density contrast and h is the height of the plume. For a
975 plume 10 km tall, explaining 300 m-tall uplifts would require a plume/environment density
976 difference of $\sim 30 \text{ kg m}^{-3}$, which could occur if the plume-environment salinity difference
977 were $\sim 5\text{--}10\%$ (*Pappalardo and Barr* 2004), marginally consistent with current estimates of
978 the salinity of Europa’s ocean (cf. *McKinnon and Zolensky* 2003; *Hand and Chyba* 2007).
979 However, as pointed out by *Showman and Han* (2004), it is difficult to understand how
980 strong compositional contrasts can be maintained against mixing if the shell is convecting.
981 Furthermore, any partial melting in the ice would tend to deplete the ice shell of salts
982 (which percolate down into the ocean with the melt), so maintaining such compositional
983 density contrasts over long timescales is difficult (*Showman and Han* 2004). *Pappalardo and*
984 *Barr* (2004) proposed that the compositional convection is a transient process that begins
985 with a recent onset of thermal convection and then dies off as the ice shell becomes depleted
986 in salts. If so, then the uplifts would be short-lived and would disappear as the shell became
987 salt-free. However, they also suggested that diking from the base of the ice shell might
988 replenish the shell with salts.

989 *Han and Showman* (2005) performed two-dimensional numerical simulations of thermo-
990 compositional convection to test the qualitative scenario of *Pappalardo and Barr* (2004).
991 Because grid-based methods can cause an artificial numerical diffusion of the salinity, *Han*
992 *and Showman* (2005) treated the salinity using the Particle-In-Cell method, which allows
993 advection of the salt with essentially no numerical diffusion. Following *Pappalardo and*
994 *Barr* (2004), they initialized the simulations with a warm salt-poor ice layer underlying a
995 colder, saltier, denser ice layer. In typical simulations, a Rayleigh-Taylor instability devel-
996 oped between the salt-poor and saltier layers, leading to compositionally driven diapirs that

997 generated pits and uplifts with topography of ~ 300 m or more (see Figure 4). Because the
998 instability involves the relatively cold near-surface ice, it occurs over a timescale $\eta_0\chi/(g\delta\Delta\rho)$,
999 where η_0 is the melting-temperature viscosity, χ is the assumed viscosity contrast across the
1000 ice shell, δ is the thickness of the salty layer, and $\Delta\rho$ is the density difference between
1001 the salty and salt-poor layers. This leads to pit-and-uplift formation timescales less than
1002 Europa’s known surface age of 30–100 Myr (*Zahnle et al.* 2003) only for viscosity contrasts
1003 $< 10^7$ – 10^8 . For viscosity contrasts $> 10^8$, pits and uplifts cannot form in timescales less than
1004 Europa’s surface age. The implication is that compositional convection can only produce
1005 Europa’s pits and uplifts if Europa’s surface is weak. The simulated pits and uplifts were
1006 10–30 km wide (see Figure 4); explaining the many pits and uplifts with diameters < 5 km
1007 is difficult.

1008 As described above, matching the observed sizes of pits and uplifts remains a challenge.
1009 Pits and uplifts range in diameter from ~ 3 –50 km (*Greenberg et al.* 2003; *Spaun* 2002;
1010 *Rathbun et al.* 1998). Based on an early sampling of Galileo images, *Pappalardo et al.* (1998)
1011 suggested that a preferred diameter of ~ 10 km exists, which *Spaun* (2002) and *Spaun et al.*
1012 (2004) revised downward to ~ 4 –8 km after performing an exhaustive survey of images that
1013 became available later in the mission. *Greenberg et al.* (2003) also performed an exhaustive
1014 survey and suggested that, when a preferred diameter exists at all, it is ~ 3 km and reflects
1015 the limits of image resolution rather than a physical peak. However, these divergent results
1016 may reflect differences in analysis methods rather than an actual discrepancy (see *Goodman*
1017 *et al.* 2004, Appendix A). For our purposes, the main point is that, regardless of the preferred
1018 diameter, many pits and uplifts are small, with diameters of 3–10 km. Although convection
1019 (with salinity) can plausibly produce the largest of these features, explaining the smallest
1020 (3–5 km-diameter) features is difficult. It is plausible that multiple origins exist for pits and
1021 uplifts, with some of the larger features resulting from convection and the smallest features
1022 resulting from some other process.

1023

5.2. Chaos

1024 Based on observations of Europa’s chaos terrains, several authors have proposed that
 1025 chaos results from convection within the ice shell, possibly aided by partial melting (*Pap-*
 1026 *palaro et al.* 1998; *Head and Pappalardo* 1999; *Collins et al.* 2000; *Figueredo et al.* 2002;
 1027 *Spaun* 2002; *Schenk and Pappalardo* 2004; *Spaun et al.* 2004). Here we review theoretical
 1028 work that investigates whether convection can lead to surface disruption and whether that
 1029 disruption has the properties of chaos (see also chapter by Collins and Nimmo).

1030

5.2.1. Runaway heating in convective plumes

1031 Motivated by the suggestion that the disaggregation and tilting of chaos blocks would
 1032 be aided by partial melting under the lithosphere (*Collins et al.* 2000), several authors have
 1033 proposed that runaway tidal heating and localized partial melting occurs within warm, as-
 1034 cending convective plumes, promoting the formation of chaos (*Wang and Stevenson* 2000;
 1035 *Sotin et al.* 2002; *Tobie et al.* 2003) (see also chapter by Collins and Nimmo). This attrac-
 1036 tive idea is based on the temperature-dependence of the Maxwell model for tidal heating
 1037 (equation 5), which predicts that tidal heating increases strongly with temperature at low
 1038 temperature (scaling as η^{-1}) and decreases strongly with temperature at high temperature
 1039 (scaling as η), peaking at intermediate values corresponding to $\omega\tau_M \sim 1$ (at temperatures of
 1040 220 to 270 K for melting-temperature viscosities of 10^{12} to 10^{15} Pa s). The low-temperature
 1041 behavior promotes runaway: increases in temperature enhance the tidal heating rate, leading
 1042 to further increases in temperature. For ice grain sizes exceeding ~ 0.5 mm (i.e., melting-
 1043 temperature viscosities $\geq 10^{14}$ Pa s), the peak heating occurs at temperatures exceeding the
 1044 melting temperature, which suggests that under appropriate conditions this runaway can
 1045 drive temperatures all the way to the melting temperature within a localized, ascending
 1046 warm plume.

1047

While the idea merits further investigation, several possible roadblocks exist. First,

1048 calculations by *Tobie et al.* (2003) and *Nimmo and Giese* (2005) suggest that melting the
1049 near-surface ice (at 1–3 km depth) is difficult because of the high power generation that is
1050 required. *Tobie et al.* (2003)’s tidally heated convection simulations, for example, produce
1051 partial melting only at depths exceeding 10 km, which may be too deep to allow disaggrega-
1052 tion of the surface.

1053 A potentially more serious issue is that for ice grain sizes < 0.5 mm, the Maxwell model
1054 (equation 5) predicts that the runaway changes sign near the melting temperature. *Tobie*
1055 *et al.* (2003) and *Mitri and Showman* (2005) point out that if the melting-temperature
1056 viscosity is 10^{13} Pa s or less (implying ice grain sizes of ≤ 0.1 mm), then for plausible ice-shell
1057 temperatures, the greatest tidal heating occurs in *cold* plumes, *not* the warm plumes (see their
1058 Figure 3). In this case, warm plumes would be heated *less* than the background ice, implying
1059 a negative feedback that reduces the thermal contrasts of plumes relative to the background.
1060 This would effectively preclude runaway heating in warm plumes. Given the small viscosities
1061 and grain sizes apparently required to explain pits and uplifts via convection (*Nimmo and*
1062 *Manga* 2002; *Showman and Han* 2004), this difficulty is relatively serious. However, the
1063 problem might be surmounted in the presence of low-eutectic-temperature contaminants
1064 (sulfuric acid or chloride salts), which could allow melting at sufficiently low temperatures
1065 for the positive feedback to operate up to the (lowered) melting temperature. Whether large
1066 pockets of melt would result (sufficient to float the overlying chaos blocks, as suggested by
1067 *Collins et al.* (2000)) would depend on the concentration of the impurities.

1068 Finally, the Maxwell model used in convection studies to date (*Wang and Stevenson*
1069 *2000*; *Sotin et al.* 2002; *Tobie et al.* 2003), which is essentially that of equation (5), is
1070 rigorously appropriate to an ice shell that exhibits no lateral variation in viscosity (i.e., it
1071 is a “zero-dimensional” Maxwell model). However, it is unclear whether this is appropriate
1072 for the heterogeneous conditions of Europa’s ice shell. A warm plume surrounded by colder,
1073 stiffer ice may exhibit cyclical tidal stress and strain patterns (hence dissipation as a function
1074 of temperature) different from those used to derive equation (5). *Moore* (2001) argued
1075 that small-scale structures such as convective plumes would not couple well to the large

1076 (hemispheric) scale of the tidal flexing, and that, as a result, minimal lateral variation in the
1077 tidal heating rate across convective plumes could occur. If so, the local runaways envisioned
1078 by *Wang and Stevenson (2000)*, *Sotin et al. (2002)*, and *Tobie et al. (2003)* would be ruled
1079 out. More detailed analyses are needed to clarify this issue.

1080 *Mitri and Showman (2008b)* revisited this issue with a two-dimensional model corre-
1081 sponding to a horizontal cross-section through a cylindrical, vertically oriented plume. A
1082 Maxwell viscoelastic rheology was adopted; the plume and environment were allowed to take
1083 different viscosities and elastic parameters. Given an imposed cyclical tidal-flexing stress and
1084 strain field at infinity, *Mitri and Showman (2008b)* solved for the stress, strain, and tidal
1085 dissipation within and surrounding the plume. These calculations showed that tidal dissi-
1086 pation does remain strongly temperature-dependent inside a convective plume (even when
1087 the background temperature is held constant), broadly supporting the idea that plumes can
1088 experience positive (or negative) feedbacks between local temperature and local tidal heating
1089 rate. Nevertheless, it would be worthwhile to extend these calculations to 3D and explore a
1090 broader range of geometries.

1091 In summary, theoretical work to date supports the idea that tidal dissipation depends
1092 strongly on temperature in a convective plume, but whether the tidal heating in hot plumes
1093 is larger or smaller than the background heating rate depends on the ice grain size. Near
1094 the melting temperature, positive feedbacks (runaways) are possible for large grain sizes, but
1095 negative feedbacks occur for small grain sizes.

1096 5.2.2. *The difficulty of fracturing the surface*

1097 Thermal convection causes typical stresses of $10^{-3} - 10^{-2}$ MPa, which is much smaller
1098 than the $\sim 1-3$ MPa failure strength of unfractured ice. This discrepancy raises difficulties
1099 for understanding how solid-state convection can induce surface disruption.

1100 However, several factors could ameliorate this difficulty. First, Europa's surface shows

1101 abundant evidence that *tidal* stresses, which reach ~ 0.1 MPa at Europa’s current eccen-
 1102 tricity, have fractured the surface (*Greenberg et al.* 1998; *Hoppa et al.* 1999). For example,
 1103 models for the formation of Europa’s cycloidal ridges suggest a fracture yield stress of just
 1104 0.04 MPa (*Hoppa et al.* 1999). Field studies on the Ross Ice Shelf, one of Earth’s closest
 1105 analogs to Europa’s ice shell, also exhibit failure strengths of order 0.1 MPa (*Kehle* 1964).
 1106 While not definitive, these studies are consistent with the idea that Europa’s near-surface ice
 1107 is weak, but it is not clear whether these estimates are appropriate for the failure of Europa’s
 1108 entire lithosphere. If, for example, cycloids are relatively shallow phenomena, the relatively
 1109 low stress associated with cycloid propagation may be relevant to Europa’s near-surface ice
 1110 only. If Europa’s band topography forms in a manner similar to terrestrial mid-ocean ridges
 1111 (*Prockter et al.* 2002), the yield strength of Europa’s lithosphere at the time and location
 1112 of band formation is ~ 0.4 to 2 MPa (*Stempel et al.* 2005). Another approach may be to
 1113 consider the effects of microcracking on the rheology of near-surface ice (*Tobie et al.* 2004).
 1114 Between a depth a ~ 15 to 40 km on Earth, microcracks are expected to play a role in
 1115 accommodating deformation, and facilitate semi-brittle/plastic behavior that is conducive
 1116 to forming zones of weakness in the crust (*Kohlstedt et al.* 1995; *Tackley* 2000a; *Bercovici*
 1117 2003b). Further field characterization of relevant terrestrial analogs and studies of flexure
 1118 and failure on Europa constrained by new spacecraft data are needed to shed light upon this
 1119 issue.

1120 Second, *Showman and Han* (2005) pointed out that stresses can become greatly en-
 1121 hanced within a thin “stress boundary layer” near the surface, promoting the likelihood of
 1122 surface fracture. This phenomenon results from the need to balance forces in a lithosphere
 1123 whose width far exceeds its thickness (*Melosh* 1977; *Fowler* 1985, 1993; *McKinnon* 1998;
 1124 *Solomatov* 2004a,b). To illustrate, consider a two-dimensional lithosphere with horizontal
 1125 dimension x and vertical dimension z . Horizontal force balance in the lithosphere leads to
 1126 the stress equilibrium condition

$$\frac{\partial \sigma_{xx}}{\partial x} + \frac{\partial \sigma_{xz}}{\partial z} = 0 \tag{33}$$

1128 where σ_{xx} and σ_{xz} are the horizontal normal and shear stresses, respectively. The shear stress

1129 is zero at the surface but due to convection (or other processes) is nonzero in the interior.
1130 Suppose the shear stress at the base of the stress boundary layer is σ_b . For a stress boundary
1131 layer of thickness h that experiences this shear stress over a horizontal distance L , we have
1132 to order-of-magnitude

$$1133 \quad \sigma_{xx} \sim \frac{L}{h} \sigma_b. \quad (34)$$

1134 The appropriate value for h is the viscosity scale height in the lithosphere (*Solomatov 2004a*),
1135 which is ~ 1 km for European conditions. The interior convective stresses should remain
1136 coherent over distances L comparable to the inter-plume spacing, which is similar to the ice-
1137 shell thickness. Adopting $L \sim 20$ km, we thus see that stresses can become enhanced by a
1138 factor of ~ 20 within the stress boundary layer. In agreement with this estimate, numerical
1139 simulations by *Showman and Han (2005)* show that, although convective stresses within
1140 the ice-shell interior are typically $\sim 10^{-3}$ – 10^{-2} MPa, the normal stresses due to thermal
1141 convection can exceed ~ 0.1 MPa near the surface.

1142 Third, the stresses that occur during compositional convection in a heterogeneous salty
1143 ice shell would far exceed those due to thermal convection alone. For the density contrasts
1144 needed to explain ~ 300 m-tall uplifts ($\Delta\rho \sim 30 \text{ kg m}^{-3}$ over a height range $h \sim 10$ km),
1145 typical convective stresses are $\sim \Delta\rho gh \sim 0.4$ MPa. In the presence of a stress boundary
1146 layer, near-surface stresses could be enhanced by an additional order of magnitude or more.
1147 These values exceed those needed to fracture ice. Thus, the idea that convection can fracture
1148 the surface seems reasonable.

1149 *5.2.3. Can convection produce a chaos-like morphology?*

1150 To test the hypothesis that convection can cause formation of chaos-type terrains, *Show-*
1151 *man and Han (2005)* performed two-dimensional numerical simulations of thermal convection
1152 in Europa's ice shell including the effects of plasticity, which is a continuum representation
1153 for deformation by brittle failure. Plastic deformation occurs when the deviatoric stresses
1154 reach a specified yield stress σ_Y ; at lower stresses, the rheology corresponds to a Newtonian,

1155 temperature-dependent viscosity (cf. *Trompert and Hansen 1998; Moresi and Solomatov*
1156 *1998; Tackley 2000b*). Partial melting and salinity were not considered. These simulations
1157 showed four regimes of behavior depending on the yield stress, thickness of the ice shell,
1158 and other parameters. At large yield stresses (≥ 0.1 MPa), the stresses never attain nec-
1159 essary values for plastic deformation, and so stagnant-lid convection occurs. At modestly
1160 smaller yield stresses (~ 0.03 – 0.08 MPa), a thick, cold upper lid remains, but it deforms via
1161 plastic deformation (see Figure 5). *Showman and Han (2005)* dubbed this the “pliable lid”
1162 regime. Most of the plastic deformation is confined near the surface, as a result of the stress
1163 boundary layer. At even smaller yield stresses (< 0.05 MPa), the convection moves away
1164 from stagnant-lid regime, exhibiting either episodic foundering and regrowth of the lid (see
1165 Figure 6) or continual recycling of the lid.

1166 What is the connection between these simulations and Europa’s chaos terrains? The
1167 formation of chaos requires not only surface fracture but sufficient strains to rotate/translate
1168 surviving chaos rafts and disaggregate the intervening matrix. Yet the existence of chaos
1169 rafts suggests that, in many cases, surface materials remained near the surface even as they
1170 were disrupted. Thus, modes of deformation involving complete foundering of the upper lid
1171 (e.g., Figure 6) appear not to have occurred on Europa. On the other hand, the so-called
1172 “pliable lid” regime of *Showman and Han (2005)* (Figure 5) seems to capture key aspects of
1173 the observed behavior. In these simulations, the near-surface strain rates exceed 10^{-14} sec $^{-1}$
1174 in localized regions, implying that order-unity strains would occur on timescales of several
1175 Myr. This is sufficient to disaggregate the surface. The absence of foundering in these
1176 simulations suggests that chaos rafts would remain at the surface, as observed. Interestingly,
1177 these high-strain regions were localized, occurring in zones only ~ 5 km wide. This is an
1178 encouraging result, although the simulations must be extended to 3D to determine whether
1179 the disrupted regions would have quasi-circular rather than linear (band-like) morphology.
1180 However, a difficulty is that the pliable-lid regime occurs over only a narrow range of yield
1181 stresses; a yield stress that is slightly too large or small pushes the behavior into stagnant-lid
1182 or lithospheric-foundering regimes, respectively. Potentially, partial-melting or porosity in

1183 the subsurface could cause a density stratification that would prevent lithospheric foundering
1184 (*Collins et al.* 2000) and allow the observed behavior to occur over a wider range of yield
1185 stresses.

1186 Although thermal and/or compositional convection seems to be a viable mechanism for
1187 causing at least some chaos terrains, explaining the specific observed aspects of Europa's
1188 chaos remains a challenge. A cautionary note is provided by attempts to simulate Earth's
1189 plate tectonics from first principles, which show that the interaction of convection with
1190 brittle deformation can depend sensitively on the adopted formulation for the brittle rheology
1191 (*Tackley* 2000a,b,c; *Bercovici* 2003a). One may expect similar sensitivity in the interaction of
1192 convection with brittle deformation on Europa. A full understanding of whether, and how,
1193 convection can cause chaos terrains will require future numerical studies that investigate
1194 compositional effects, partial melting, and a wider range of brittle rheologies.

1195 6. Discussion

1196 Despite many advances in the knowledge of ice rheology, the behavior of solid-state
1197 convection, and the interaction between convection and lithospheric deformation, several
1198 aspects of the behavior of Europa's ice shell remain unexplained. Here, we describe several
1199 key gaps in knowledge about Europa, which are required to address the fundamental ques-
1200 tions about Europa's ice shell posed in §1: Can Europa's ice shell convect at present? How
1201 does tidal dissipation affect convection? Can convection drive resurfacing? What role does
1202 compositional heterogeneity play in driving motion in Europa's shell?

- 1203 • *What is the thickness and thermal structure of Europa's ice shell?* Further spacecraft
1204 data are needed to constrain the true thickness of Europa's ice shell, to characterize the
1205 topography inferred to form from convection (at both short and long wavelengths), and
1206 to determine the thermal structure of the ice shell (namely, the depth to warm ice).
1207 Global geophysical data obtained by an orbiter equipped with, for example, a laser

1208 altimeter, radar sounder, a near-infrared mapping spectrometer, and high-resolution
1209 imaging system are needed to answer many of the basic questions posed above. Such
1210 data would also provide constraints for more sophisticated modeling efforts suggested
1211 below.

- 1212 • *Can convection cause resurfacing?* Models published to date provide encouragement
1213 that at least some fraction of Europa's pits, uplifts, and chaos could result from con-
1214 vection in the ice shell, but the models are nevertheless far from explaining the actual
1215 observed properties of these features. Compositional convection allows pits and uplifts
1216 with the observed topography to be produced, but the simulated features are wider
1217 than most of Europa's pits and uplifts unless ice viscosities are extremely small. Con-
1218 vection models including simple parameterizations of brittle failure can produce some
1219 chaos-like behaviors, but they also produce behaviors that appear not to occur on Eu-
1220 ropa. A new generation of three-dimensional models including salinity, partial melting,
1221 and more realistic parameterizations of brittle failure can help determine whether pits,
1222 uplifts, and chaos can actually result from convection.
- 1223 • *How does tidal flexing on Europa affect the microphysical structure and rheological*
1224 *behavior of ice?* It is not known how the cyclical tidal flexing of Europa's ice shell
1225 affects the ice in its interior. The Maxwell model is perhaps an overly simplistic
1226 description of the behavior of Europa's ice. For example, we suggest that a model of
1227 transient creep may be more appropriate description of cyclically deformed ice
1228 than the currently used steady-state creep model. Laboratory experiments are needed
1229 to clarify how tidal dissipation occurs on a microphysical scale in ice, and to clarify
1230 whether cyclical flexing affects ice microstructure.
- 1231 • *How does tidal flexing interact with mechanical, thermal, and compositional hetero-*
1232 *geneity in the ice shell?* Implicit in our discussion of the effects of tidal flexing on heat
1233 transfer has been the assumption that tidal dissipation is heterogeneous, and that tidal
1234 heating obeys the Maxwell model (equation 5). The results of laboratory experiments
1235 must be combined with sophisticated geophysical techniques to study the localization

1236 of tidal strain and heating in model european ice shells with thermal, mechanical, and
1237 compositional heterogeneity to more accurately model tidal dissipation and its link to
1238 resurfacing.

1239 **Acknowledgements:** Author Barr acknowledges support from the Southwest Research
1240 Institute and NASA OPR Grant NNG05GI15G to W. B. McKinnon. Author Showman
1241 acknowledges support from NASA PG&G grant NNX07AR27G. We thank G. Tobie, W. B.
1242 McKinnon, and an anonymous reviewer for helpful comments.

REFERENCES

1243

1244 Alley, R. B., J. H. Peralto, and C. R. Bentley, Grain growth in polar ice: I. Theory,
1245 *Journal of Glaciology*, *32*, 415–424, 1986a.

1246 Alley, R. B., J. H. Peralto, and C. R. Bentley, Grain growth in polar ice: II. Application,
1247 *Journal of Glaciology*, *32*, 425–433, 1986b.

1248 Barnes, P. R. F., R. Mulvaney, K. Robinson, and E. W. Wolff, Observations of polar ice from
1249 the Holocene and the glacial period using the scanning electron microscope, *Annals*
1250 *of Glaciology*, *35*, 559–566, 2002.

1251 Barr, A. C., Mobile lid convection beneath Enceladus' south polar terrain, in press, *J.*
1252 *Geophys. Res.*, doi:10.1029/2008JE003114, 2008.

1253 Barr, A. C., and W. B. McKinnon, Convection in ice I shells and mantles with self-consistent
1254 grain size, *J. Geophys. Res.*, *112*, E02012, doi:10.1029/2006JE002781, 2007.

1255 Barr, A. C., and R. T. Pappalardo, Onset of convection in the icy Galilean satellites: Influ-
1256 ence of rheology, *J. Geophys. Res.*, *110*, E12005, doi:10.1029/2004JE002371, 2005.

1257 Barr, A. C., R. T. Pappalardo, and S. Zhong, Convective instability in ice I with non-
1258 Newtonian rheology: Application to the icy Galilean satellites, *J. Geophys. Res.*, *109*,
1259 E12008, doi:10.1029/2004JE002296, 2004.

1260 Bercovici, D., Frontiers: The generation of plate tectonics from mantle convection, *Earth and*
1261 *Planetary Science Letters*, *205*, 107–121, doi:10.1016/S0012-821X(02)01009-9, 2003a.

1262 Bercovici, D., The generation of plate tectonics form mantle convection, *Earth Planet. Sci.*
1263 *Lett.*, *205*, 107–121, 2003b.

1264 Birger, B. I., Rheology of the Earth and a thermoconvective mechanism for sedimentary
1265 basin formaiton, *Geophys. J. Int.*, *134*, 1–12, 1998.

- 1266 Birger, B. I., Excitation of thermoconvective waves in the continental lithosphere, *Geophys.*
1267 *J. Int.*, *140*, 24–36, 2000.
- 1268 Budd, W. F., and T. H. Jacka, A review of ice rheology for ice sheet modelling, *Cold Regions*
1269 *Science and Technology*, *16*, 107–144, 1989.
- 1270 Carlson, R. W., M. S. Anderson, R. Mehlman, and R. E. Johnson, Distribution of hydrate
1271 on Europa: Further evidence for sulfuric acid hydrate, *Icarus*, *177*, 461–471, doi:
1272 10.1016/j.icarus.2005.03.026, 2005.
- 1273 Carr, M. H., et al., Evidence for a subsurface ocean on Europa, *Nature*, *391*, 363–365, 1998.
- 1274 Cassen, P., R. T. Reynolds, and S. J. Peale, Is there liquid water on Europa, *Geophys. Res.*
1275 *Lett.*, *6*, 731–734, 1979.
- 1276 Cassen, P., S. J. Peale, and R. T. Reynolds, Tidal dissipation in Europa - A correction,
1277 *Geophys. Res. Lett.*, *7*, 987–988, 1980.
- 1278 Chandrasekhar, S., *Hydrodynamic and Hydromagnetic Stability*, International Series of
1279 Monographs on Physics, Oxford: Clarendon, 1961.
- 1280 Collins, G. C., J. W. Head, R. T. Pappalardo, and N. A. Spaul, Evaluation of models for
1281 the formation of chaotic terrain on Europa, *J. Geophys. Res.*, *105*, 1709–1716, 2000.
- 1282 Consolmagno, G. J., and J. S. Lewis, The Evolution of Icy Satellite Interiors and Surfaces,
1283 *Icarus*, *34*, 280–293, 1978.
- 1284 De Bresser, J. H. P., C. J. Peach, J. P. J. Reijs, and C. J. Spiers, On dynamic recrystallization
1285 during solid state flow: Effects of stress and temperature, *Geophys. Res. Lett.*, *25*,
1286 3457–3460, 1998.
- 1287 De La Chapelle, S., O. Castelnau, V. Lipenkov, and P. Duval, Dynamic recrystallization and
1288 texture development in ice as revealed by the study of deep ice cores in Antarctica
1289 and Greenland, *J. Geophys. Res.*, *103*, 5091–5106, 1998.

- 1290 Derby, B., The Dependence of Grain Size on Stress During Dynamic Recrystallization, *Acta*
1291 *Metall. Mater.*, *39*, 955–962, 1991.
- 1292 Dumoulin, C., M.-P. Doin, and L. Fleitout, Heat transport in stagnant lid convection with
1293 temperature- and pressure-dependent Newtonian or non-Newtonian rheology, *J. Geophys. Res.*, *104*,
1294 12,759–12,777, 1999.
- 1295 Durand, G., et al., Effect of impurities on grain growth in cold ice sheets, *J. Geophys. Res.*,
1296 *111*, F01015, doi:10.1029/2005JF000320, 2006.
- 1297 Durham, W. B., and L. A. Stern, Rheological properties of water ice – Applications to
1298 satellites of the outer planets, *Ann. Rev. Earth Planet Sci.*, *29*, 295–330, 2001.
- 1299 Durham, W. B., S. H. Kirby, and L. A. Stern, Effect of Dispersed Particulates on the
1300 Rheology of Water Ice at Planetary Conditions, *J. Geophys. Res.*, *97*, 20,883–20,897,
1301 1992.
- 1302 Durham, W. B., S. H. Kirby, and L. A. Stern, Flow of Ices in the Ammonia-Water System,
1303 *J. Geophys. Res.*, *98*, 17,667–17,682, 1993.
- 1304 Durham, W. B., L. A. Stern, and S. H. Kirby, Rheology of ice I at low stress and elevated
1305 confining pressure, *J. Geophys. Res.*, *106*, 11,031–11,042, 2001.
- 1306 Durham, W. B., L. A. Stern, T. Kubo, and S. H. Kirby, Flow strength of highly hydrated Mg-
1307 and Na-sulfate hydrate salts, pure and in mixtures with water ice, with application
1308 to Europa, *J. Geophys. Res.*, *110*, E12,010, doi:10.1029/2005JE002475, 2005.
- 1309 Duval, P., and M. Montagnat, Comment on “Superplastic deformation of ice: Experimental
1310 observations” by D. L. Goldsby and D. L. Kohlstedt, *J. Geophys. Res.*, *107*, 2082,
1311 doi:10.1029/2002JB001842, 2002.
- 1312 Duval, P., L. Arnaud, O. Brissaud, M. Montagnat, and S. de La Chapelle, Deformation
1313 and recrystallization processes of ice from polar ice sheets, *Annals of Glaciology*, *30*,
1314 83–87, 2000.

- 1315 Fagents, S. A., Considerations for effusive cryovolcanism on Europa: The post-Galileo per-
1316 spective, *J. Geophys. Res.*, *108*, 5139, doi:10.1029/2003JE002128, 2003.
- 1317 Figueredo, P. H., and R. Greeley, Resurfacing history of Europa from pole-to-pole ge-
1318 ologimapping, *Icarus*, *167*, 287–312, doi:10.1016/j.icarus.2003.09.016, 2004.
- 1319 Figueredo, P. H., F. C. Chuang, J. Rathbun, R. L. Kirk, and R. Greeley, Geology and
1320 origin of Europa’s “Mitten” feature (Murias Chaos), *J. Geophys. Res.*, *107*, 5026,
1321 doi:10.1029/2001JE001591, 2002.
- 1322 Fowler, A. C., Fast thermoviscous convection, *Stud. Appl. Math.*, *72*, 189–219, 1985.
- 1323 Fowler, A. C., Boundary layer theory and subduction, *J. Geophys. Res.*, *98*, 21,997–22,005,
1324 1993.
- 1325 Freeman, J., L. Moresi, and D. A. May, Thermal convection with a water ice I
1326 rheology: Implications for icy satellite evolution, *Icarus*, *180*, 251–264, doi:
1327 10.1016/j.icarus.2005.07.014, 2006.
- 1328 Glen, J. W., The creep of polycrystalline ice, *Proc. Royal Soc. London, Series A*, *228*, 519–
1329 538, 1955.
- 1330 Goldsby, D. L., Diffusion Creep of Ice: Constraints from Laboratory Creep Experiments, ab-
1331 stract number 2186, in *Lunar and Planetary Institute Conference Abstracts XXXVIII*,
1332 vol. 38, Lunar and Planetary Institute, Houston, Tex., 2007.
- 1333 Goldsby, D. L., and D. L. Kohlstedt, Superplastic deformation of ice: Experimental obser-
1334 vations, *J. Geophys. Res.*, *106*, 11,017–11,030, 2001.
- 1335 Goldsby, D. L., and D. L. Kohlstedt, Reply to comment by P. Duval and M. Montagnat on
1336 “Superplastic deformation of ice: Experimental observations”, *J. Geophys. Res.*, *107*,
1337 2313, doi:10.1029/2002JB001842, 2002.
- 1338 Goodman, D. J., H. J. Frost, and M. F. Ashby, The plasticity of polycrystalline ice, *Phi-*
1339 *los. Mag. A*, *43*, 665–695, 1981.

- 1340 Goodman, J. C., G. C. Collins, J. Marshall, and R. T. Pierrehumbert, Hydrothermal plume
1341 dynamics on Europa: Implications for chaos formation, *J. Geophys. Res.*, *109*, 3008,
1342 doi:10.1029/2003JE002073, 2004.
- 1343 Greeley, R., et al., Europa: Initial Galileo Geological Observations, *Icarus*, *135*, 4–24, 1998.
- 1344 Greeley, R. C., C. Chyba, J. W. Head, T. McCord, W. B. McKinnon, and R. T. Pappalardo,
1345 Geology of Europa, in *Jupiter: The Planet, Satellites & Magnetosphere*, pp. 329–362,
1346 Cambridge University Press, New York, 2004.
- 1347 Greenberg, R., G. V. Hoppa, B. R. Tufts, P. Geissler, J. Riley, and S. Kadel, Chaos on
1348 Europa, *Icarus*, *141*, 263–286, doi:10.1006/icar.1999.6187, 1999.
- 1349 Greenberg, R., M. A. Leake, G. V. Hoppa, and B. R. Tufts, Pits and uplifts on Europa,
1350 *Icarus*, *161*, 102–126, doi:10.1016/S0019-1035(02)00013-1, 2003.
- 1351 Greenberg, R., et al., Tectonic Processes on Europa: Tidal Stresses, Mechanical Response,
1352 and Visible Features, *Icarus*, *135*, 64–78, doi:10.1006/icar.1998.5986, 1998.
- 1353 Han, L., and A. P. Showman, Thermo-compositional convection in Europa’s icy shell with
1354 salinity, *Geophys. Res. Lett.*, *32*, L20201, doi:10.1029/2005GL023979, 2005.
- 1355 Han, L., and A. P. Showman, Implications of shear heating and fracture zones for ridge
1356 formation on Europa, *Geophys. Res. Lett.*, *35*, L03202, doi:10.1029/2007GL031957,
1357 2008.
- 1358 Hand, K. P., and C. F. Chyba, Empirical constraints on the salinity of the european ocean and
1359 implications for a thin ice shell, *Icarus*, *189*, 424–438, doi:10.1016/j.icarus.2007.02.002,
1360 2007.
- 1361 Head, J. W., III, and R. T. Pappalardo, Brine mobilization during lithospheric heating
1362 on Europa: Implications for formation of chaos terrain, lenticula texture, and color
1363 variations, *J. Geophys. Res.*, *104*, 27,143–27,155, 1999.

- 1364 Hoppa, G. V., B. R. Tufts, R. Greenberg, and P. E. Geissler, Formation of cycloidal features
1365 on Europa, *Science*, *285*, 1899–1902, 1999.
- 1366 Hussmann, H., and T. Spohn, Thermal-orbital evolution of Io and Europa, *Icarus*, *171*,
1367 391–410, doi:10.1016/j.icarus.2004.05.020, 2004.
- 1368 Hussmann, H., T. Spohn, and K. Wiczerkowski, Thermal Equilibrium States of Europa’s
1369 Ice Shell: Implications for Internal Ocean Thickness and Surface Heat Flow, *Icarus*,
1370 *156*, 143–151, doi:10.1006/icar.2001.6776, 2002.
- 1371 Kehle, R. O., Deformation of the Ross Ice Shelf, Antarctica., *Geol. Soc. Amer. Bull.*, *75*,
1372 259–286, 1964.
- 1373 Kirk, R. L., and D. J. Stevenson, Thermal evolution of a differentiated Ganymede and
1374 implications for surface features, *Icarus*, *69*, 91–134, 1987.
- 1375 Kohlstedt, D. L., B. Evans, and S. J. Mackwell, Strength of the lithosphere: Constraints
1376 imposed by laboratory experiments, *J. Geophys. Res.*, *100*, 17,587–17,602, 1995.
- 1377 Manga, M., and D. Weeraratne, Experimental study of non-Boussinesq Rayleigh-Bénard
1378 convection at high Rayleigh and Prandtl numbers, *Physics of Fluids*, *11*, 2969–2976,
1379 doi:10.1063/1.870156, 1999.
- 1380 McCarthy, C., D. L. Goldsby, and R. F. Cooper, Transient and Steady-State Creep Re-
1381 sponses of Ice-I/Magnesium Sulfate Hydrate Eutectic Aggregates, in *Lunar and Plan-*
1382 *etary Institute Conference Abstracts, Lunar and Planetary Institute Conference Ab-*
1383 *stracts*, vol. 38, p. abs. no. 2429, 2007.
- 1384 McCord, T. B., et al., Hydrated salt minerals on Europa’s surface from the Galileo near-
1385 infrared mapping spectrometer (NIMS) investigation, *J. Geophys. Res.*, *104*, 11,827–
1386 11,852, 1999.
- 1387 McKinnon, W., Geodynamics of icy satellites, in *Solar System Ices*, pp. 525–550, Kulwer,
1388 Dordrecht, 1998.

- 1389 McKinnon, W. B., Convective instability in Europa's floating ice shell, *Geophys. Res. Lett.*,
1390 26, 951–954, 1999.
- 1391 McKinnon, W. B., On convection in ice I shells of outer solar system bodies, with specific
1392 application to Callisto, *Icarus*, 183, 435–450, 2006.
- 1393 McKinnon, W. B., and M. E. Zolensky, Sulfate Content of Europa's Ocean and Shell: Evo-
1394 lutionary Considerations and Some Geological and Astrobiological Implications, *As-
1395 trobology*, 3, 879–897, doi:10.1089/153110703322736150, 2003.
- 1396 Melosh, H. J., Shear stress on the base of a lithospheric plate, *Pure and Applied Geophysics*,
1397 115, 429–439, doi:10.1007/BF01637119, 1977.
- 1398 Melosh, H. J., A. G. Ekholm, A. P. Showman, and R. D. Lorenz, The temperature of Europa's
1399 subsurface water ocean, *Icarus*, 168, 498–502, doi:10.1016/j.icarus.2003.11.026, 2004.
- 1400 Mitri, G., and A. P. Showman, Convective-conductive transitions and sensitivity of a con-
1401 vecting ice shell to perturbations in heat flux and tidal-heating rate: Implications for
1402 Europa, *Icarus*, 177, 447–460, 2005.
- 1403 Mitri, G., and A. P. Showman, Thermal convection in ice-I shells of Titan and Enceladus,
1404 *Icarus*, 193, 387–396, doi:10.1016/j.icarus.2007.07.016, 2008a.
- 1405 Mitri, G., and A. P. Showman, A model for the temperature-dependence of tidal dissipation
1406 in convective plumes on icy satellites: Implications for Europa and Enceladus, *Icarus*,
1407 195, 758–764, doi:10.1016/j.icarus.2008.01.010, 2008b.
- 1408 Montagnat, M., and P. Duval, Rate controlling processes in the creep of polar ice, influence of
1409 grain boundary migration associated with recrystallization, *Earth Planet. Sci. Lett.*,
1410 183, 179–186, 2000.
- 1411 Moore, W. B., Coupling Tidal Dissipation and Convection, abstract number 37.03,
1412 *AAS/Division for Planetary Sciences Meeting*, 33, 2001.

- 1413 Moore, W. B., Thermal equilibrium in Europa's ice shell, *Icarus*, *180*, 141–146, doi:
1414 10.1016/j.icarus.2005.09.005, 2006.
- 1415 Moore, W. B., and G. Schubert, The tidal response of Europa, *Icarus*, *147*, 317–319, 2000.
- 1416 Moresi, L.-N., and V. S. Solomatov, Mantle convection with a brittle lithosphere: thoughts
1417 on the global tectonic styles of Earth and Venus, *Geophys. J. Int.*, *133*, 669–682, 1998.
- 1418 Nimmo, F., Stresses generated in cooling viscoelastic ice shells: Application to Europa, *J.*
1419 *Geophys. Res.*, *109*, E12001, doi:10.1029/2004JE002347, 2004.
- 1420 Nimmo, F., and B. Giese, Thermal and topographic tests of Europa chaos formation models
1421 from Galileo E15 observations, *Icarus*, *177*, 327–340, doi:10.1016/j.icarus.2004.10.034,
1422 2005.
- 1423 Nimmo, F., and M. Manga, Causes, characteristics, and consequences of convective diapirism
1424 on Europa, *Geophys. Res. Lett.*, *29*, 2109, doi:10.1029/2002GL015754, 2002.
- 1425 Nimmo, F., and R. T. Pappalardo, Diapir-induced reorientation of Saturn's moon Enceladus,
1426 *Nature*, *441*, 614–616, doi:10.1038/nature04821, 2006.
- 1427 Nimmo, F., R. T. Pappalardo, and B. Giese, On the origins of band topography, Europa,
1428 *Icarus*, *166*, 21–32, doi:10.1016/S0019-1035(03)00236-7, 2003.
- 1429 O'Brien, D. P., P. Geissler, and R. Greenberg, A Melt-through Model for Chaos Formation
1430 on Europa, *Icarus*, *156*, 152–161, 2002.
- 1431 Ojakangas, G. W., and D. J. Stevenson, Thermal state of an ice shell on Europa, *Icarus*, *81*,
1432 220–241, 1989.
- 1433 Pappalardo, R. T., and A. C. Barr, The origin of domes on Europa: The role of
1434 thermally induced compositional diapirism, *Geophys. Res. Lett.*, *31*, L01701, doi:
1435 10.1029/2003GL019202, 2004.

- 1436 Pappalardo, R. T., S. J. Reynolds, and R. Greeley, Extensional tilt blocks on Miranda:
1437 Evidence for an upwelling origin of Arden Corona, *J. Geophys. Res.*, *102*, 13,369–
1438 13,380, doi:10.1029/97JE00802, 1997.
- 1439 Pappalardo, R. T., et al., Geological evidence for solid-state convection in Europa's ice shell,
1440 *Nature*, *391*, 365–368, 1998.
- 1441 Peltier, W. R., D. L. Goldsby, D. L. Kohlstedt, and L. Tarasov, Ice-age ice-sheet rheology:
1442 constraints from the Last Glacial Maximum form of the Laurentide ice sheet, *Annals*
1443 *of Glaciology*, *vol.30*, pp.163-176, *30*, 163–176, 2000.
- 1444 Petrenko, V. F., and R. W. Whitworth, *Physics of Ice*, Oxford University Press, New York,
1445 1999.
- 1446 Poirier, J.-P., *Creep of Crystals*, Cambridge, UK: Cambridge University Press, 1985.
- 1447 Prockter, L. M., J. W. Head, R. T. Pappalardo, R. J. Sullivan, A. E. Clifton, B. Giese,
1448 R. Wagner, and G. Neukum, Morphology of European bands at high resolu-
1449 tion: A mid-ocean ridge-type rift mechanism, *J. Geophys. Res.*, *107*, 5028, doi:
1450 10.1029/2000JE001458, 2002.
- 1451 Ranalli, G., *Rheology of The Earth: Deformation and Flow Processes in Geophysics and*
1452 *Geodynamics*, Allen & Unwin, Inc., Boston, 1987.
- 1453 Rathbun, J. A., G. S. Musser, and S. W. Squyres, Ice diapirs on Europa: Implications for
1454 liquid water, *Geophys. Res. Lett.*, *25*, 4157–4160, doi:10.1029/1998GL900135, 1998.
- 1455 Reynolds, R. T., and P. M. Cassen, On the internal structure of the major satellites of the
1456 outer planets, *Geophys. Res. Lett.*, *6*, 121–124, 1979.
- 1457 Ruiz, J., and R. Tejero, Heat flow, lenticulae spacing, and possibility of convection in the ice
1458 shell of Europa, *Icarus*, *162*, 362–373, 2003.
- 1459 Schenk, P., and M. P. A. Jackson, Diapirism on Triton - A record of crustal layering and
1460 instability, *Geology*, *21*, 299–302, 1993.

- 1461 Schenk, P. M., and R. T. Pappalardo, Topographic variations in chaos on Eu-
1462 ropa: Implications for diapiric formation, *Geophys. Res. Lett.*, *31*, L16703, doi:
1463 10.1029/2004GL019978, 2004.
- 1464 Schmeling, H., On the interaction between small- and large-scale convection and postglacial
1465 rebound flow in a power-law mantle, *Earth Planet. Sci. Lett.*, *84*, 254–262, 1987.
- 1466 Schmidt, K. G., and D. Dahl-Jensen, An ice crystal model for Jupiter’s moon Europa, *Ann.*
1467 *Glaciology*, *37*, 129–133, 2003.
- 1468 Schubert, G., D. L. Turcotte, and P. Olson, *Mantle Convection in the Earth and Planets*,
1469 Cambridge University Press, New York, 2001.
- 1470 Shimizu, I., Stress and temperature dependence of recrystallized grain size: A subgrain mis-
1471 orientation model, *Geophys. Res. Lett.*, *25*, 4237–4240, doi:10.1029/1998GL900136,
1472 1998.
- 1473 Showman, A. P., and L. Han, Numerical simulations of convection in Europa’s ice shell: Im-
1474 plications for surface features, *J. Geophys. Res.*, E01010, doi:10.1029/2003JE002103,
1475 2004.
- 1476 Showman, A. P., and L. Han, Effects of plasticity on convection in an ice shell: Implications
1477 for Europa, *Icarus*, *177*, 425–437, doi:10.1016/j.icarus.2005.02.020, 2005.
- 1478 Solomatov, V. S., Scaling of temperature- and stress-dependent viscosity convection, *Physics*
1479 *of Fluids*, *7*, 266–274, 1995.
- 1480 Solomatov, V. S., Initiation of subduction by small-scale convection, *J. Geophys. Res.*, *109*,
1481 B01412, doi:10.1029/2003JB002628, 2004a.
- 1482 Solomatov, V. S., Correction to “Initiation of subduction by small-scale convection”, *J.*
1483 *Geophys. Res.*, *109*, B05,408, doi:10.1029/2004JB003143, 2004b.
- 1484 Solomatov, V. S., and A. C. Barr, Onset of convection in fluids with strongly temperature-
1485 dependent, power-law viscosity, *Phys. Earth. Planet. Interiors*, *155*, 140–145, 2006.

- 1486 Solomatov, V. S., and A. C. Barr, Onset of convection in fluids with strongly temperature-
1487 dependent, power-law viscosity 2. Dependence on the initial perturbation, *Phys.*
1488 *Earth. Planet. Interiors*, *165*, 1–13, 2007.
- 1489 Solomatov, V. S., and L.-N. Moresi, Scaling of time-dependent stagnant lid convection: Ap-
1490 plication to small-scale convection on Earth and other terrestrial planets, *J. Geophys.*
1491 *Res.*, *105*, 21,795–21,818, 2000.
- 1492 Sotin, C., J. W. Head, and G. Tobie, Europa: Tidal heating of upwelling thermal plumes
1493 and the origin of lenticulae and chaos melting, *Geophys. Res. Lett.*, *29*, 1233, doi:
1494 10.1029/2001GL013844, 2002.
- 1495 Spaun, N. A., Chaos, lenticulae, and lineae on Europa: Implications for geological history,
1496 crustal thickness, and the presence of an ocean, Ph.D. thesis, Brown University, 2002.
- 1497 Spaun, N. A., J. W. Head, III, and R. T. Pappalardo, European Chaos and Lenticulae: A
1498 Synthesis of Size, Spacing, and Areal Density Analyses, abstract number 1409, in
1499 *Lunar and Planetary Institute Conference Abstracts XXXV*, vol. 35, 2004.
- 1500 Spohn, T., and G. Schubert, Oceans in the icy Galilean satellites of Jupiter?, *Icarus*, *161*,
1501 456–467, 2003.
- 1502 Stempel, M. M., A. C. Barr, and R. T. Pappalardo, Model constraints on the opening rates
1503 of bands on Europa, *Icarus*, *177*, 297–304, 2005.
- 1504 Stengel, K. C., D. C. Oliver, and J. R. Booker, Onset of convection in a variable viscosity
1505 fluid, *Journal of Fluid Mechanics*, *120*, 411–431, 1982.
- 1506 Tackley, P. J., Mantle Convection and Plate Tectonics: Toward an Integrated Physical and
1507 Chemical Theory, *Science*, *288*, 2002–2007, 2000a.
- 1508 Tackley, P. J., Self-consistent generation of tectonic plates in time-dependent, three-
1509 dimensional mantle convection simulations: 1. Pseudoplastic yielding, *Geochem. Geo-*
1510 *phys. Geosyst.*, *1*, doi:10.1029/2000GC000036, 2000b.

- 1511 Tackley, P. J., Self-consistent generation of tectonic plates in time-dependent, three-
1512 dimensional mantle convection simulations: 2. Strain weakening and asthenosphere,
1513 *Geochem. Geophys. Geosyst.*, *1*, doi:10.1029/2000GC000043, 2000c.
- 1514 Thorsteinsson, T., J. Kipfstuhl, and H. Miller, Textures and fabrics in the GRIP ice core, *J.*
1515 *Geophys. Res.*, *102*, 26,583–26,600, doi:10.1029/97JC00161, 1997.
- 1516 Tobie, G., G. Choblet, and C. Sotin, Tidally heated convection: Constraints on Europa’s ice
1517 shell thickness, *J. Geophys. Res.*, *108*, 5124, doi:10.1029/2003JE002099, 2003.
- 1518 Tobie, G., G. Choblet, J. Lunine, and C. Sotin, Interaction between the convective sublayer
1519 and the cold fractured surface of Europa’s ice shell, in *Workshop on Europa’s Icy*
1520 *Shell: Past, Present, and Future*, p. 7033, 2004.
- 1521 Trompert, R., and U. Hansen, Mantle convection simulations with rheologies that generate
1522 plate-like behaviour, *Nature*, *395*, 686–689, 1998.
- 1523 Turcotte, D. L., and G. Schubert, *Geodynamics: Applications of Continuum Physics to*
1524 *Geological Problems*, John Wiley & Sons, New York, 2002.
- 1525 Wang, H., and D. J. Stevenson, Convection and internal melting of Europa’s ice shell, ab-
1526 stract number 1293, in *Lunar and Planetary Institute Conference Abstracts XXXI*,
1527 Lunar and Planetary Institute, Houston, Tex., 2000.
- 1528 Weertman, J., Creep deformation of ice, *Ann. Rev. Earth Planet Sci.*, *11*, 215–240, 1983.
- 1529 Weiss, J., J. Vidot, M. Gay, L. Arnaud, P. Duval, and J. R. Petit, Dome Concordia ice
1530 microstructure: impurities effect on grain growth, *Annals of Glaciology*, *35*, 552–558,
1531 2002.
- 1532 Zahnle, K., P. Schenk, H. Levison, and L. Dones, Cratering rates in the outer Solar System,
1533 *Icarus*, *163*, 263–289, doi:10.1016/S0019-1035(03)00048-4, 2003.
- 1534 Zimmer, C., K. K. Khurana, and M. G. Kivelson, Subsurface oceans on Europa and Callisto:
1535 Constraints from Galileo magnetometer observations, *Icarus*, *147*, 329–347, 2000.

1536 Zolotov, M. Y., and E. L. Shock, Composition and stability of salts on the surface
1537 of Europa and their oceanic origin, *J. Geophys. Res.*, *106*, 32,815–32,828, doi:
1538 10.1029/2000JE001413, 2001.

Table I.: Rheological Parameters for Ice I after *Goldsby and Kohlstedt (2001)*.

Parameter	Basal Slip	Grain Boundary Sliding	Dislocation Creep
B ($\text{m}^p \text{Pa}^{-n} \text{s}^{-1}$)	2.2×10^{-7}	6.2×10^{-14}	4.0×10^{-19}
n	2.4	1.8	4.0
p	0	1.4	0
Q^* (kJ mol $^{-1}$)	60	49	60

Parameter	Name	Volume Diffusion
V_m (m 3 mol $^{-1}$)	Molar volume	1.97×10^{-5}
b (m)	Burger's vector	4.52×10^{-10}
δ (m) = $2b$	Grain boundary width	9.04×10^{-10}
$D_{o,v}$ (m 2 s $^{-1}$)	Volume diffusion constant	9.10×10^{-4}
Q_v^* (kJ mol $^{-1}$)	Volume diffusion activation energy	59.4
$D_{o,b}$ (m 2 s $^{-1}$)	GB diffusion constant	7.0×10^{-4}
Q_b^* (kJ mol $^{-1}$)	GB diffusion activation energy	49

Table II.: Critical Rayleigh Numbers For Stopping and Starting Convection in a Newtonian Ice Shell (after *Solomatov and Barr (2007)*)

$\log_{10}(\Delta\eta)$	Equivalent θ	Ra_{cr}^*	$Nu(Ra_{cr}^*)$	$Ra_{cr,1}$	$Nu(Ra_{cr,1})$
5	11.5	2.7×10^5	1.30	3.67×10^5	1.56
8	18.4	1.35×10^6	1.22	2.41×10^6	1.53
10	23.0	2.94×10^6	1.19	5.88×10^6	1.49
12	27.6	5.61×10^6	1.17	1.218×10^7	1.47
16	36.8	1.58×10^7	1.14	3.59×10^7	1.43
20	46	3.57×10^7	1.12	9.40×10^7	1.40

Fig. 1.— Deformation maps for ice I using the rheology of *Goldsby and Kohlstedt* (2001), for ice with grain sizes of 1.0 cm, 1.0 mm, and 0.1 mm. Lines on the deformation map represent the transition stress between mechanisms as a function of temperature. From *Barr et al.* (2004).

Fig. 2.— (a) Schematic temperature structures for a conductive (top) and convective (bottom) ice shell on Europa (from *Mitri and Showman* 2005). (b) Values of ice shell thickness where convection is possible in Europa’s ice shell as a function of grain size. For ice grain sizes $d > 2$ mm, deformation during the onset of convection is accommodated largely by GSS creep (black), but for smaller grain sizes, deformation is accommodated by volume diffusion (gray). After *Barr and Pappalardo* (2005). (c) Behavior of an ice shell in Ra - Nu space during the onset of convection in a basally heated fluid with $\theta = 18$ ($\Delta\eta = 10^8$) (black arrows) and decay of convection (gray arrows). Diamonds illustrate location of simulations of the onset of convection by *Mitri and Showman* (2005), points, solid, dashed lines show locations of simulations of the decay of convection by *Solomatov and Barr* (2007). When convection begins, Nu jumps from 1 to ~ 1.6 - 1.7 (see §4.2.3), depending on the form of temperature perturbation used. When convection stops, Nu can achieve very low values for $Ra < Ra_{cr,1}$, but ultimately stops when $Ra < Ra_{cr}^*$, when $Nu \sim 1.1 - 1.3$ for rheological parameters for ice. (d) Heat flux as a function of ice shell thickness for equilibrium configurations of Europa’s ice shell, illustrating the jump in heat flux at the convective/conductive transition $D \sim 9$ km. Tidal heating with a tidal-flexing strain amplitude 2×10^{-5} is assumed, and a Newtonian rheology is used with a melting-temperature viscosity of 10^{13} Pa s and a viscosity contrast of 10^6 . Triangles and diamonds show heat flux into the bottom and out the top of the ice shell, respectively. Solid curve shows relationship between flux and thickness for a conductive solution with no tidal heating. From *Mitri and Showman* (2005).

Fig. 3.— Temperature (a,c) and dynamic topography (b,d) from simulations of thermal convection in a 50 km-thick European ice shell from *Showman and Han* (2004). Rheology is Newtonian with $Q^* = 60 \text{ kJ mol}^{-1}$, $\eta_o = 10^{13} \text{ Pa s}$ (right), and $\eta_o = 10^{14} \text{ Pa s}$ (left), and upper viscosity cutoff of $10^9 \eta_o$. (a,b) A high melting point viscosity leads to sluggish convection beneath a thick stagnant lid, and topography of order tens of meters, much lower than observed on Europa. Domain is 150 km wide and 50 km deep. (c,d) Convection in an ice shell melting point viscosity of 10^{13} Pa s leads to vigorous convection characterized by narrow upwellings and a thinner stagnant lid. Domain is 300 km wide by 50 km deep. Although the topography predicted by more vigorous convection has a smaller wavelength, the plume buoyancy is unchanged between the two cases: the dynamic topography is \sim tens of meters.

Fig. 4.— (a) Topography, (b) composition, and (c) temperature for a numerical simulation of convection with salinity from *Han and Showman* (2005). Domain is 45 km wide and 15 km thick. Black dots in (b) are tracers marking the locations of salt-poor, low-density ice, which was initially near the bottom of the ice shell but experiences diapirism. White regions are salty, denser ice. The topography attains 200–300 m with widths of 15–20 km. This suggests that Europa’s widest pits and uplifts can form from convection with salinity.

Fig. 5.— Simulation of pure thermal convection including plasticity from *Showman and Han* (2005) with a yield stress of 0.03 MPa. Temperature divided by melting temperature (top), two-dimensional velocity (second), second invariant of strain rate (third), and surface velocity (bottom). Domain is 45 km wide and 15 km deep. Plastic deformation occurs in the upper lid, leading to significant surface deformation. This may be relevant to chaos formation on Europa.

Fig. 6.— A time sequence (top to bottom) of a simulation of pure thermal convection including plasticity from *Showman and Han* (2005) with a yield stress of 0.03 MPa. This simulation illustrates necking and overturn of the upper lid, followed by reformation of a cold upper lid by conduction.

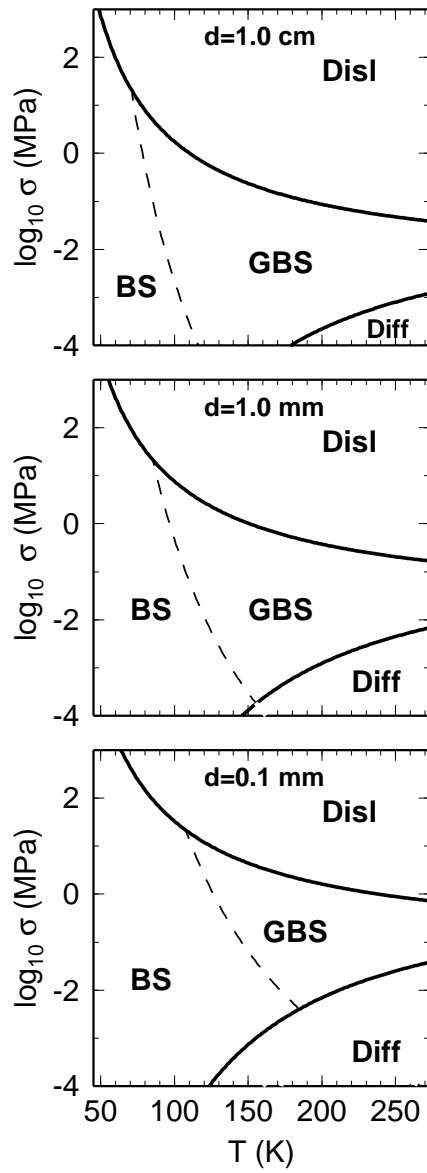


Fig. 1.

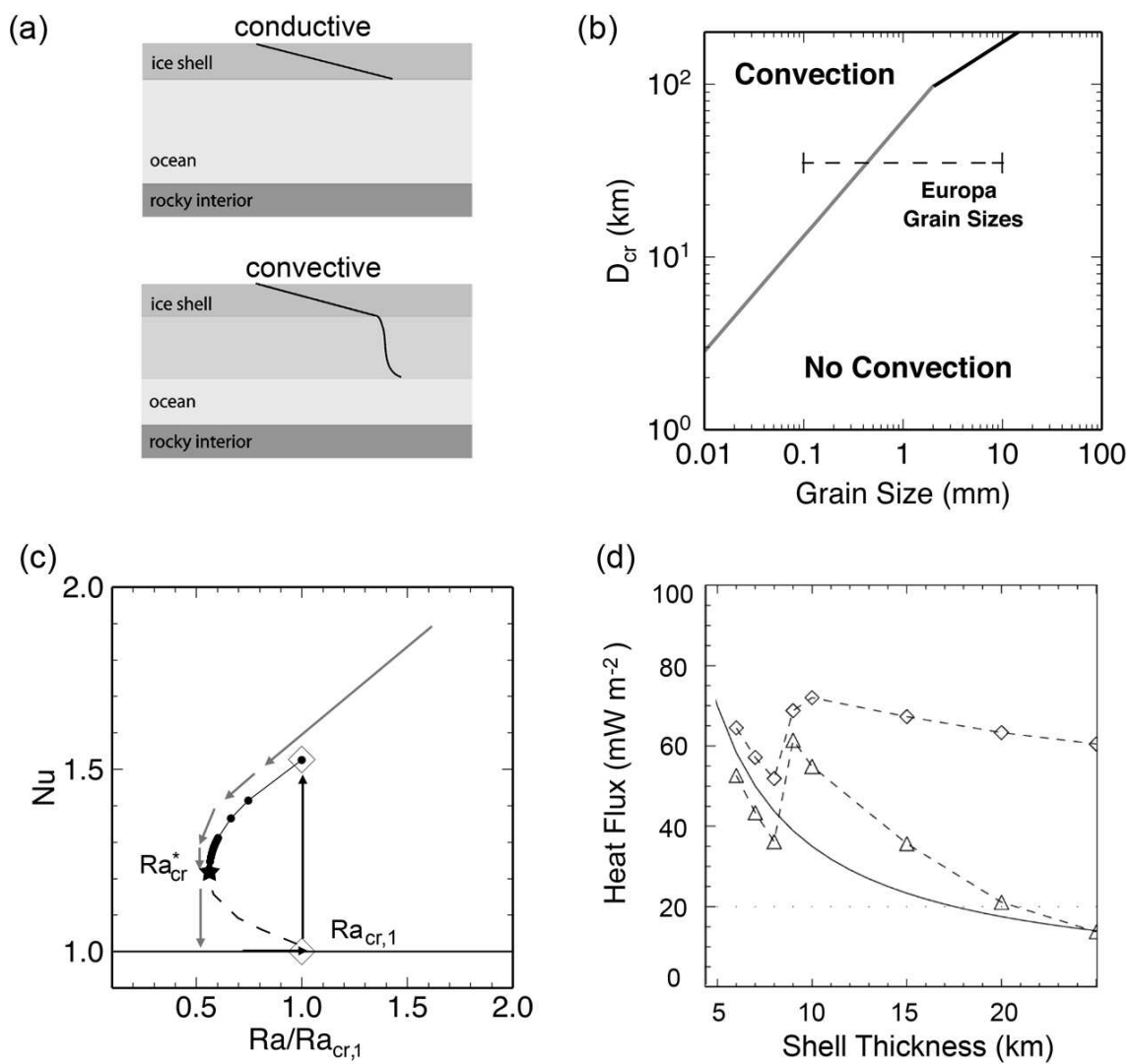


Fig. 2.

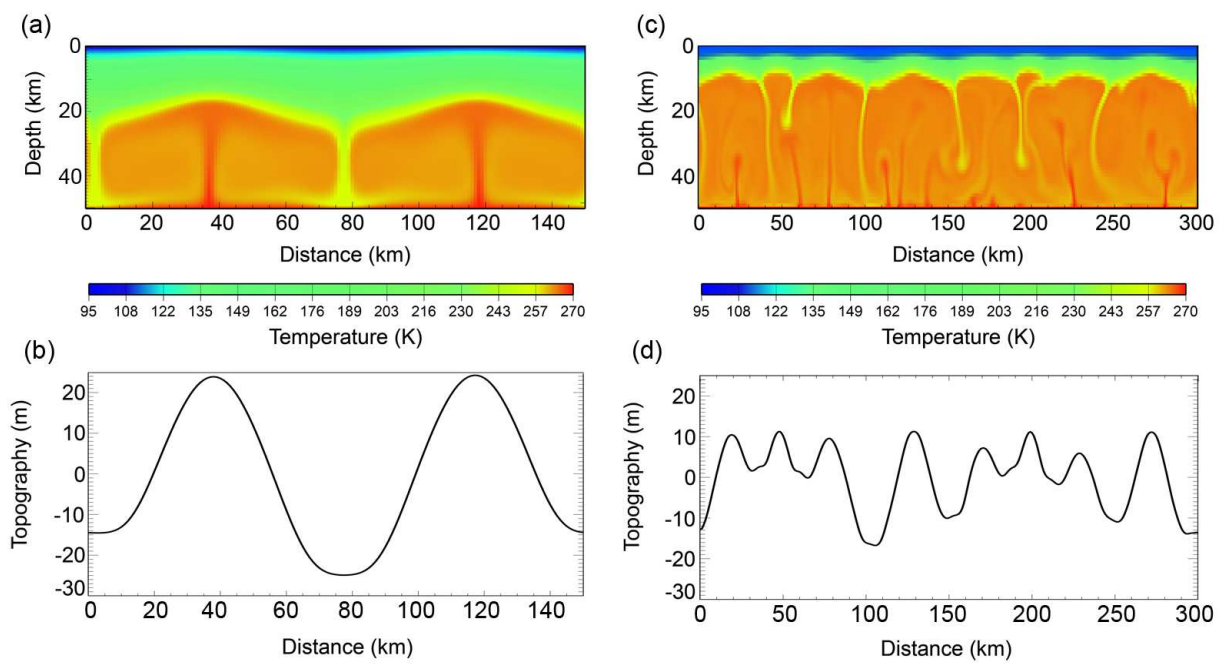


Fig. 3.

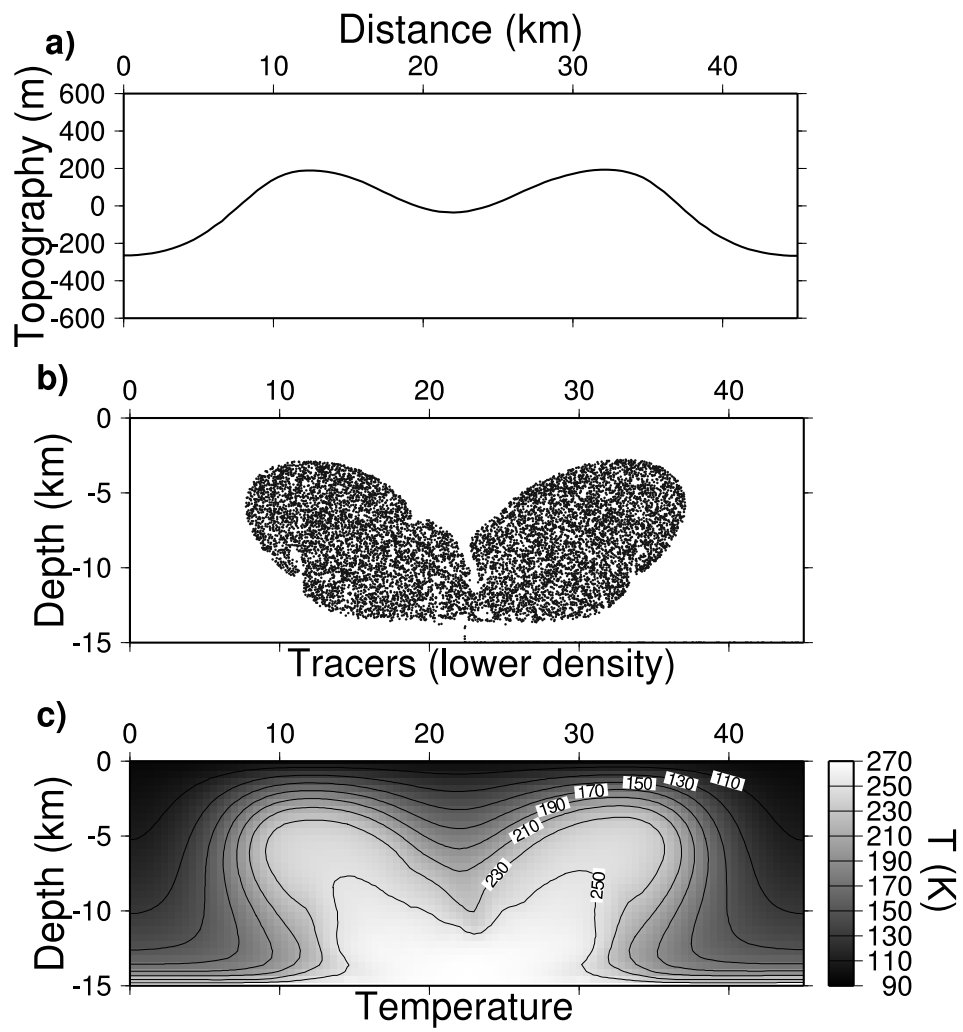


Fig. 4.

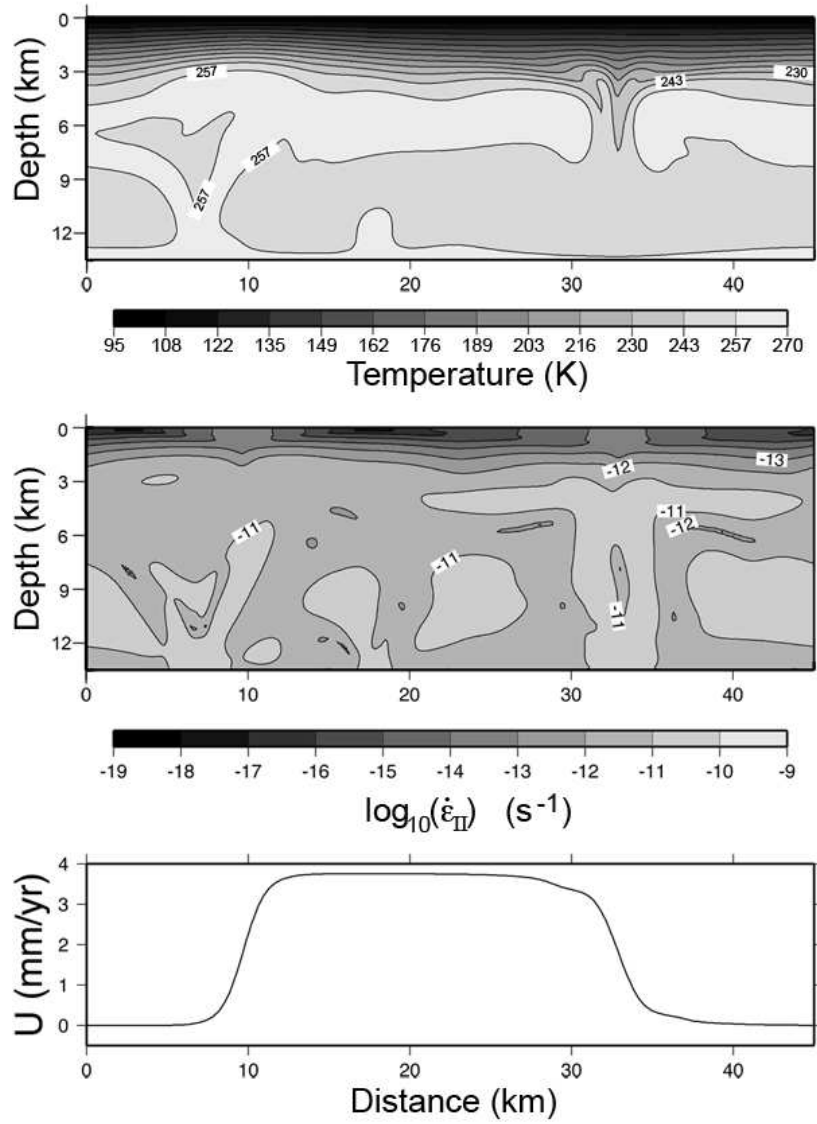


Fig. 5.

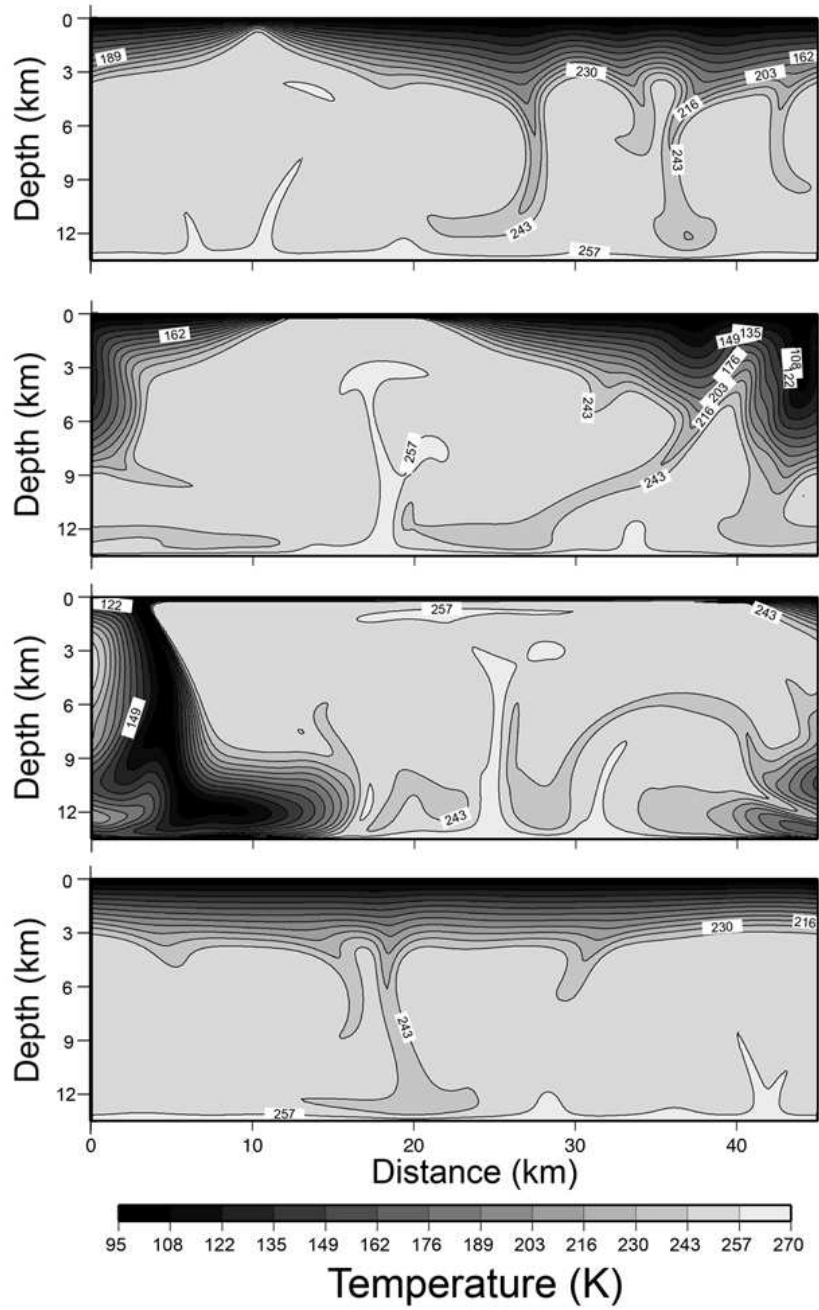


Fig. 6.